Desalination 447 (2018) 55–73

Contents lists available at ScienceDirect

Desalination

journal homepage: www.elsevier.com/locate/desal

Energy matrices, exergoeconomic and enviroeconomic analysis of modified multi–wick basin type double slope solar still

Piyush Pal[a,*], Rahul Dev[a], Dhananjay Singh[b], Amimul Ahsan[c,d]

[a] Department of Mechanical Engineering, Motilal Nehru National Institute of Technology Allahabad, Allahabad 211004, Uttar Pradesh, India
[b] Department of Chemical Engineering, Institute of Engineering & Technology Lucknow, Lucknow 226021, Uttar Pradesh, India
[c] Department of Civil and Construction Engineering, Swinburne University of Technology, Melbourne, Australia
[d] Department of Civil Engineering, Uttara University, Dhaka 1230, Bangladesh

ARTICLE INFO

Keywords:
Energy matrices
Exergoeconomic analysis
Multi–wick solar still
Solar energy

ABSTRACT

The present study is devoted to developing a thermal model of modified multi–wick basin type double slope solar still (MMWBDSSS). Analytical expressions of temperatures of water, wick, walls, and glass covers, distillate yield and instantaneous efficiency have been derived. The experimental validation of thermal model has been carried out and a fair agreement has been detected between theoretical results and experimental observations. On the basis of annual energy and exergy, the energy matrices, namely, the energy payback time (EPBT); life cycle conversion efficiency (LCCE); energy production factor (EPF), enviroeconomic and exergoeconomic analysis has also been evaluated for the solar still with jute and black cotton wicks under the climatic conditions of Allahabad, Uttar Pradesh (U.P.), India. The CO_2 emission mitigated per annum has been found to be 7.82 and 8.69 tons on energy basis; and 0.155 and 0.198 tons on exergy basis with jute and black cotton wicks at 1 cm water depth, respectively. The exergoeconomic parameter has been found to be 0.0623 kWh/Rs. and 0.0791 kWh/Rs. for the solar still with jute and black cotton wicks at 1 cm water depth, respectively for 4% interest rate and 50 years life span of the system.

1. Introduction

Water scarcity has become a worldwide critical issue in most of the territories of the globe in last four–five decades. Rapid industrialization and economic development, exponential population growth, over–-exploitation of forest resources brought up serious consequences for the mankind. A nearly 97.5% of the water body is covered by seawater, potable water only constitutes 0.014% of total available water on earth [1]. About 60% of the globe's population will face water shortage by the year 2025 due to excessive use of natural and groundwater resources which is primarily a source of potable or drinkable water [2]. Conventional desalination technologies are available for purifying the water, but due to high energy intensive and dependent on fossils fuels, carbon emission to the environment degrade ecology and natural habitats [3].

Therefore, finding renewable and sustainable energy technology, which is cost–effective, safe, environmentally friendly to produce potable water from unkempt or toxic water for its optimal use in drinking and other purposes is utmost necessary. Solar thermal energy based solar distillation looks promising and one of the recognized renewable source for distilling brackish water in remote, arid, local and rural regions with near zero emission of carbon to the environment. The solar distillation occurred in a house type structure called solar still. Solar still further categorize into (i) passive solar stills, and (ii) active solar stills. Many researchers have worked on different designs and configurations of passive solar stills to increase the distillate yield and overall performance such as: double effect solar distiller [4], hemispherical solar distiller [5], triangular solar still [6], double basin double slope solar distiller [7], effect of air flow on 'V' type solar distiller [8], conical solar still [9], stepped solar distiller [10], weir–type cascade solar distiller with energy storage system [11], tubular solar still [12–14], point–focus parabolic solar still [15], portable solar still with thermoelectric module [16,17], single basin fin–type solar still [18,19], solar still with corrugated absorbers [20], solar distiller with internal and external reflectors [21,22], effect of air motion inside the solar still [23,24]. Rufuss et al. [25] summarized a detailed review in focus of active; passive; and multi–effect solar stills, described the modifications for enhancing the distillate output using fins, heat storage systems, condensers and stated optimization schemes for increasing the heat and mass transfer rates inside the solar distillers. Many studies have

* Corresponding author.
E-mail addresses: rme1454@mnnit.ac.in, piyushpal19@gmail.com (P. Pal), rahuldsurya@mnnit.ac.in (R. Dev).

https://doi.org/10.1016/j.desal.2018.09.006
Received 18 April 2018; Received in revised form 19 July 2018; Accepted 7 September 2018

Nomenclature

A_b	Basin area (m^2)
A_E	East wall area (m^2)
A_{Eg}	East glass cover area (m^2)
A_N	North wall area (m^2)
A_S	South wall area (m^2)
A_W	West wall area (m^2)
A_{Wg}	West glass cover area (m^2)
C	Specific heat of water (J/Kg–K)
$\frac{dT_w}{dt}$	Change in the water temperature in small time dt
E_{in}	Embodied energy (kWh)
$E_{ex,\ ann}$	Annual exergy gain (kWh)
$E_{out,\ ann}$	Annual solar energy output (kWh)
$E_{sol(en),\ ann}$	Annual solar energy retrieved by the solar still (kWh)
$E_{sol(ex),\ ann}$	Annual solar exergy of the solar still (kWh)
Ex	Exergy (kWh)
h_{acro}	Overall heat transfer coefficient from inner surface of acrylic wall to ambient (W/m^2–K)
h_{ba}	Heat transfer coefficient from basin to ambient air (W/m^2–K)
h_{bw}	Heat transfer coefficient from basin to water (W/m^2–K)
h_{FRPo}	Overall heat transfer coefficient from inner surface of FRP wall to ambient (W/m^2–K)
h_{go}	Overall heat transfer coefficient from inner surface of glass cover to ambient (W/m^2–K)
h_{Kacr}	Conductive heat transfer coefficient of acrylic wall (W/m^2–K)
h_{KFRP}	Conductive heat transfer coefficient of FRP wall (W/m^2–K)
h_{Kg}	Conductive heat transfer coefficient of glass cover (W/m^2–K)
h_o	Convective radiative heat transfer coefficient from outer surface of glass cover to ambient (W/m^2–K)
h_s	Heat transfer coefficient of side wall (W/m^2–K)
h_{NV}	Total internal heat transfer coefficient from north wall to vapor (W/m^2–K)
h_{VE}	Total internal heat transfer coefficient from vapor to east wall (W/m^2–K)
h_{VEg}	Total internal heat transfer coefficient from vapor to east glass cover (W/m^2–K)
h_{VS}	Total internal heat transfer coefficient from vapor to south wall (W/m^2–K)
h_{VW}	Total internal heat transfer coefficient from vapor to west wall (W/m^2–K)
h_{VWg}	Total internal heat transfer coefficient from vapor to west glass cover (W/m^2–K)
$h_{w-wick(E)}$	Heat transfer coefficient for east wick (W/m^2–K)
$h_{w-wick(W)}$	Heat transfer coefficient for west wick (W/m^2–K)
i	Interest rate (%)
$I(t)_{input}$	Total heat input to the solar still (W)
$I_E(t)$	Solar intensity on east wall (W/m^2)
$I_{Eg}(t)$	Solar intensity on east glass cover (W/m^2)
$I_{Ng}(t)$	Solar intensity on north wall through glass covers (W/m^2)
$I_S(t)$	Solar intensity on south wall (W/m^2)
$I_W(t)$	Solar intensity on west wall (W/m^2)
$I_{Wg}(t)$	Solar intensity on west glass cover (W/m^2)
k_{acr}	Thermal conductivity of Acrylic (W/m−K)
k_{FRP}	Thermal conductivity of FRP (W/m−K)
k_g	Thermal conductivity of glass cover (W/m−K)
L_{vap}	Latent heat of vaporization (J/Kg)
l_{acr}	Thickness of Acrylic sheet (m)
l_{FRP}	Thickness of FRP sheet (m)
l_g	Thickness of glass cover (m)
M	Mass of water (Kg)
$\dot{M}_{eEg}$	Hourly yield retrieved from east glass cover (ml)
$\dot{M}_{eS}$	Hourly yield retrieved from south wall (ml)
$\dot{M}_{eWg}$	Hourly yield retrieved from west glass cover (ml)
$\dot{M}_{ew}$	Total hourly yield of the solar still (ml)
M_s	Maintenance cost (Rs./year)
$\dot{M}_{total}$	Total daily yield of the solar still (ml)
n	Life span of solar still in years (y)
R_{ex}	Exergoeconomic parameter
SV	Salvage value (Rs.)
t	Time (h or s)
T_a	Ambient temperature (°C)
T_b	Basin temperature (°C)
T_w	Water temperature (°C)
$T_{w-wick(avg.)}$	Average temperature of strap layer of water–wick spread on east and west side (°C)
$T_{w-wick(E)}$	Temperature of water in east side wick (°C)
$T_{w-wick(W)}$	Temperature of water in west side wick (°C)
T_V	Vapor temperature (°C)
v	Wind velocity (m/s)

Greek

α'_b	Solar flux absorption factor for basin
α'_E	Solar flux absorption factor for east wall
α'_g	Solar flux absorption factor for glass cover
α'_{Ng}	Solar flux absorption factor for north wall through glass cover
α'_S	Solar flux absorption factor for south wall
α'_W	Solar flux absorption factor for west wall
α'_w	Solar flux absorption factor for water
ε_{acr}	Emissivity of acrylic wall
ε_g	Emissivity of glass cover
ε_w	Emissivity of water
θ	Inclination angle of glass cover (degree)
σ	Stephan–Boltzmann constant (W/m^2–K^4)
β	Packing factor
η_{ex}	Instantaneous exergy efficiency (hourly basis)
η_i	Instantaneous thermal energy efficiency (hourly basis)
η_O	Overall thermal efficiency of the solar still
dt	Small time interval (second)

Subscripts

a	Ambient
b	Basin
conv	Convection
E	East side
eff	Effective
en	Energy
ex	Exergy
exp.	experimental
e, evap	Evaporation
g	Glass cover
ins	instantaneous
i, insurf	Inner surface
N	North side
o	Outer
rad	Radiation
S	South side
theo	theoretical
V	Vapor
w	Water
W	West side
w–wick	Strap layer of water–wick

Abbreviation

CRF	Capital recovery factor
EPBT	Energy payback time
EPF	Energy production factor
LCCE	Life cycle conversion efficiency
NPV	Net present value
SFF	Sink fund factor
UAC	Uniform annual cost

suggested that the performance of passive solar distillers are better than the active solar distillers [26–30].

Rahbar and Esfahani [31] formulated a new equation to optimize the yield of a single slope solar still based on Chilton–Colburn analogy. A CFD simulation have been done to validate the results of Bulk–motion and Chilton–Colburn models. Authors reported that for a fixed length of a solar still, the yield increases with decrease in specific height and trend of yield was similar to the trend of convective heat transfer coefficient. Rahbar et al. [32] estimated the results of yield, heat and mass transfer coefficients based on new proposed relations with the CFD simulation results in the tubular solar still. A 200% reduction and 250% enhancement in productivity were reported, when glass cover and water temperature increases only 5 °C, respectively. Rahbar and Esfahani [33] proposed a relation ($Nu = 0.28Ra^{0.25}A^{-0.16}$) for natural convection heat transfer coefficient inside a single slope solar still based on SIMPLEC algorithm numerical model for several values of rayleigh number and aspect ratio. Authors reported that for a given aspect ratio, the heat transfer coefficient rises with rise in the rayleigh number and heat transfer coefficient decreases with enhancement in the length of recirculating zones for a fixed rayleigh number. Dev et al. [34,35] formulated the characteristics equations at steady state for single and double slope solar distillers for the composite climatic condition of New Delhi, India (latitude 28°35′ N, longitude 77°12′ E). Authors suggested that, 45° inclination angle of glass cover (based on instantaneous efficiency) and 0.01 m water depth at a 15° inclination should be taken for optimized results of single slope passive solar stills with respect to design and operational point of view, respectively [34]. Authors also reported that the non–linear characteristic curves gives more accurate results than linear characteristic curves [35]. Shukla and Sorayan [36] developed a thermal model for multi–wick solar distiller based on energy balance equations for validating the experimental results. In this work, the temperature of inner and outer glass covers have been used for estimating the internal heat transfer coefficients. Dwivedi and Tiwari [37] using different thermal models to estimate the internal heat transfer coefficients at winter and summer climatic conditions of New Delhi, India. In this study, it has been observed that the Dunkle's model gives the better results for experimental validation at 0.01, 0.02, and 0.03 m of water depth for single and double slope passive solar distillers. It has also seen that the values of internal heat transfer have a marginal variation with water depths. Al–Sulttani et al. [38] fabricated a double slope solar distiller with rubber scrapers using a 3° inclination angle of condensing glass cover to achieve the higher productivity through scrape down the accumulated condensed drops, which were falls back to the basin. In this work, convective and evaporative heat transfer coefficients have been evaluated using experimental data and then the theoretical results have been compared to demonstrate the advantages of rubber scrapers. The daily yield and total internal heat transfer coefficient has been found to be 4.24 l/m^2 day and 38.754 W/m^2 °C, respectively. The effect of water depth and glass cover inclination on the distillate yield and heat transfer coefficient have been analyzed for the climatic conditions of New Delhi, India [39]. The authors reported that the heat transfer coefficient varies with water depth and inclination of glass cover. The maximum yield was obtained at lower water depth. Sahota et al. [40] using water–based nanofluids (Al_2O_3, TiO_2 and CuO) in passive double slope solar distiller for increasing the heat transfer rates to achieve the significant distillate, energy, and exergy. Authors reported that Al_2O_3–water based nanofluid was better than TiO_2, CuO–water based nanofluid on the energy and exergy basis for the annual yield, mitigating the CO_2 emissions, and environmental cost.

Sodha et al. [41] constructed the multi–wick solar still incorporating the blackened wet jute wick and analyzed distiller's performance with the basin type solar distiller. Tiwari and Selim [42] presented the design of fibre reinforced plastic (FRP) multi–wick solar distiller and compared with simple multi–wick solar still on the basis of cost and productivity. Solar still with jute wick at an inclination angle of 10° and 40° yield more output in summer and winter season, respectively [43]. Wick–basin type solar distiller yield 85% more than basin type solar distiller and 43% more than wick type solar distiller using blackened jute cloth and 4 mm glass cover thickness [44]. Floating wick configured solar still using blackened jute wick and polystyrene sheet gives the daily output of 10.50 l/m^2 [45]. Multi–wick configured solar distillers and wick–type distiller with the effect of water flowing over the glass covers have been studied [46–49]. Various configurations of flat plate reflector with different angles from the vertical have been used in during summer, winter, spring, and autumn solstice in tilted wick type solar stills [50–54]. Concave wick solar distiller productivity and instantaneous efficiency were 200% and 50%, respectively higher than the conventional or traditional type solar still incorporating concave shape jute wick with the basin area of $1.2 \times 1.2 m^2$ and an insulation thickness of 5 cm [55]. Black cotton cloth's wick was found to be effective among jute wick, quartzite rock, sponge pieces and washed natural rock incorporating in the single basin–type double slope solar distiller with an inclination angle of 30° [56]. Pal et al. [57] designed the double slope multi–wick solar distiller using FRP and Acrylic material, in which the east, west, and south walls made transparent to enhance the heat input rate inside solar still in order to increase the productivity, nocturnal yield, and overall thermal efficiency of the system. Authors reported the 20.94% and 28.27% overall thermal efficiency (maximum) of multi–wick double slope solar still with jute and black cotton wicks, respectively. Pal et al. [58] studied the experimental and economic aspects of a modified basin–type double slope solar distiller and reported 1.94% exergy efficiency (maximum) for the system. Singh et al. [59] reported the energy matrices, exergoeconomic; annual exergy; and life cycle cost analysis for single and double slope passive solar distillers.

It could be seen from the above literature review, various methods and configurations have been incorporated to increase the water surface–condensing glass cover temperature for increasing the distillate yield and overall performance. It has also seen from the survey that the wick type solar stills in various methods give better performance than basin type solar stills for yield/m^2 in the passive mode of working. It is observed that the solar still studied in this present work have not been previously presented. In this work, a hanging multi–wick solar distiller (fabricated with FRP and Acrylic material and east, west, and south walls made transparent) have been studied on the basis of second law of thermodynamics i.e. exergy performance on annual basis, energy matrices, exergy efficiency, enviroeconomic and exergoeconomic parameters under the climatic condition of Allahabad (U.P.), India. Hence, in the present communication, a thermal model has been developed for modified multi–wick basin type double slope solar still based on the energy balance equation of different components of the system. The theoretical results of water temperature, average temperature of wicks (strap layer of water–wick), and yield have been validated with the experimental observations. Apart from this, annual exergy, energy matrices i.e. energy payback time (EPBT); energy production factor

(EPF); and life cycle conversion efficiency (LCCE), enviroeconomic (environmental cost i.e. carbon credits), and exergoeconomic analysis have also been studied for presented solar still with jute and black cotton wicks at 1 cm and 2 cm water depth under the climatic conditions of Allahabad (U.P.) (Latitude 25°27′ N & Longitude 81°44′ E), India.

2. Description of experimental setup

The experimental setup consists of a basin, glass covers, transparent walls (except north wall), and troughs for yield collection. The basin has the dimension 2 *m* × 1 *m*. Basin was constructed with the help of 5 mm thickness of Fibre Reinforced plastic (FRP), which also act as an insulation material for retarding the heat loss to the ambient environment. Basin was black colored paint from inside to increase the heat input of solar radiation and accelerate the evaporation process. In the conventional multi–wick solar stills [41,42], basin was absent to store the thermal energy of received solar radiations. The dimension of the east (E) and west (W) walls were 1 *m* × 0.12 *m*, which was fabricated with an acrylic sheet of 3 mm thickness. The dimension of the north (N) and south (S) walls has been divided into two sections. The bottom (rectangular) section, which was having a dimension of 2 *m* × 0.12 *m*, and the other (triangular) section having a height from the top or apex point of solar still to the rectangular section was 0.38 m. The total height from the top point of the solar still to the bottom is 0.50 m (the south and north wall was fabricated as a single piece, not in sections, for showing the dimensions more elaborately, section–wise dimensioning has been discussed). The south wall was fabricated with an acrylic sheet (3 mm thickness), whereas the north wall was made up of FRP (5 mm thickness), which was black painted from the inner side to enhance the solar radiation absorption rate. The concept of “equivalent thickness” has been applied for constructing the walls and basin for the same rate of heat transfer/heat loss through the solar still [57]. Two simple window glass covers of dimension 1.03 × 1.03 × 0.004 m^3 were used at an inclination angle of 15° and fixed to the solar still's frame by window putty. The window putty also acts as an insulation material for minimizing the side and top heat losses through the glass covers. Troughs were provided on walls (except north wall) to collect the yield after the evaporation–condensation process. South wall's yield was obtained through the trough (which was sticking to the south–wall), whose one end (outlet) was located on the east wall and another was located on the west wall. The condensation of glass covers was obtained through trough provided on the east and west wall, whose ends were located on the north wall. The end or outlet point of troughs were linked to the container by pipes, which guided the yield from the outlet point to the storage cylindrical vessels. Fig. 1. shows the schematic representation of modified multi–wick basin type double slope solar still.

In the present experimental setup, nineteen (19) wicks, which was hanging vertically at a distance of 10 cm (horizontal height between the two consecutive wicks) were used to facilitate the proper feeding of water to the upper or strap layer of the wick. Among the wicks, the centre wick has a maximum height of 37 cm. The pattern of remaining wicks was decreasing towards both sides of solar still and smallest height of wick (including dip portion in water) has a vertical length of 10 cm. The rods were used to hold the upper layer and vertical wicks in the proper position. The dimension of strap layer including the submerged portion in water from one side to another side was 2.02 × 0.80 × 0.001 m^3. The strap layer of wick with packing factor (β) of 0.728 provides the evaporative surface for solar still, which was 5 cm below the glass cover. With this arrangement, effective or faster evaporation can take place with more surface area prone to solar radiation. The whole structure is installed on the terrace of ‘Solar Energy Laboratory’, Department of Mechanical Engineering, MNNIT Allahabad, Allahabad, U.P. (Latitude 25°27′ N & Longitude 81°44′ E), India in the East–West direction to intercept the maximum amount of solar radiation for the whole day–length. The photograph of the solar still showing south wall's trough and pattern of hanging wicks in Fig. 2. The photograph of the solar still is shown in Fig. 3.

3. Thermal modeling

Following assumptions have been taken for the development of a thermal model of the solar still:

(a) Solar still is vapor leakage and air proof and all the processes inside

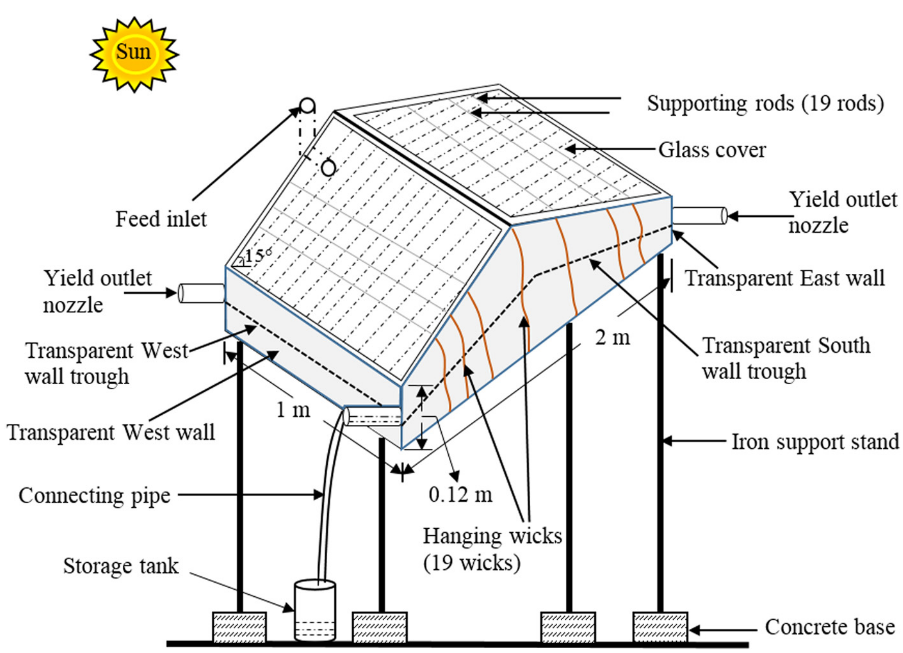

Fig. 1. Schematic diagram of modified multi–wick basin type double slope solar still.

Fig. 2. Photograph of the solar still showing south wall's trough and pattern of hanging wicks.

the system in quasi–steady state (steady state condition in the time interval, Δt).
(b) Heat capacities of the glass cover, FRP, and Acrylic is negligible.
(c) There is no temperature gradient in the water inside the basin.
(d) Heat transfer coefficients for solar still are temperature dependent.
(e) Inside solar still, a hypothetical vapor surface is considered for all the heat interactions to the surrounding surface(s).
(f) The air inside the system is assumed as humid air.
(g) The side heat loss from the walls and basin of solar still is negligible.
(h) The temperature of water in wick ($T_{w\text{–}wick}$) is slightly greater than wick's temperature (T_{wick}) i.e. $T_{w\text{–}wick} > T_{wick}$.

In the present study, solar radiation incident (i) into the basin through transparent acrylic walls, (ii) into the wick–layer through condensing glass covers, and (iii) into the basin through remaining portion of glass covers, which is not covered by wick layers below the glass covers (the area of strap layer of wicks is less than the area of glass cover). The fraction of solar flux, at different components of the solar still is mathematically expressed as [60,61]:

$$\alpha_g' = (1 - R_g)\alpha_g \quad (1)$$

$$\alpha_{Ng}' = (1 - \alpha_g)(1 - R_g)(1 - R_N)\alpha_N \quad (2)$$

$$\alpha_{wg}' = (1 - \alpha_g)(1 - R_g)(1 - R_w)\alpha_w \quad (3)$$

$$\alpha_{w-wick}' = (1 - \alpha_g)(1 - R_g)(1 - R_w)\alpha_w \quad (4)$$

$$\alpha_{bg}' = (1 - \alpha_g)(1 - R_g)(1 - R_w)(1 - \alpha_w)\alpha_b \quad (5)$$

$$\alpha_{wacr}' = (1 - \alpha_{acr})(1 - R_{acr})(1 - R_w)\alpha_w \quad (6)$$

$$\alpha_{bacr}' = (1 - \alpha_{acr})(1 - R_{acr})(1 - R_w)(1 - \alpha_w)\alpha_b \quad (7)$$

Energy balance equations for the heat transfer processes occurring for different components of the solar still is given below:

For energy balance of inner north wall surface (no solar radiation incident on north wall through east, west and south wall):

Fig. 3. Photograph of the solar still.

[Heat absorbed from radiation through glass covers]
= [Heat transfer to vapor from the inner north wall]
+ [Heat transfer from the inner surface to the outer surface of north wall]

$$\alpha'_{Ng} A_N I_{Ng}(t) = h_{NV} A_N (T_{iN} - T_V) + h_{KFRP} A_N (T_{iN} - T_{oN}) \tag{8}$$

Energy balance for outer north wall surface:

[Heat transfer from the inner surface to the outer surface of north wall]
= [Heat loss to ambient by the outer north wall]

$$h_{KFRP} A_N (T_{iN} - T_{oN}) = h_o A_N (T_{oN} - T_a) \tag{9}$$

Energy balance for inner south wall surface:

[Heat absorbed from radiation]
+ [Heat transfer from vapor to the inner south wall]
= [Heat transfer from the inner surface to the outer surface of south wall]

$$\alpha'_S A_S I_S(t) + h_{VS} A_S (T_V - T_{iS}) = h_{Kacr} A_S (T_{iS} - T_{oS}) \tag{10}$$

Energy balance for outer south wall surface:

[Heat transfer from the inner surface to the outer surface of south wall]
= [Heat loss to ambient by the outer south wall]

$$h_{Kacr} A_S (T_{iS} - T_{oS}) = h_o A_S (T_{oS} - T_a) \tag{11}$$

Energy balance for inner east wall surface:

[Heat absorbed from radiation]
+ [Heat transfer from vapor to the inner east wall]
= [Heat transfer from the inner surface to the outer surface of east wall]

$$\alpha'_E A_E I_E(t) + h_{VE} A_E (T_V - T_{iE}) = h_{Kacr} A_E (T_{iE} - T_{oE}) \tag{12}$$

Energy balance for outer east wall surface:

[Heat transfer from the inner surface to the outer surface of east wall]
= [Heat loss to ambient by the outer east wall]

$$h_{Kacr} A_E (T_{iE} - T_{oE}) = h_o A_E (T_{oE} - T_a) \tag{13}$$

Energy balance for inner west wall surface:

[Heat absorbed from radiation]
+ [Heat transfer from vapor to the inner west wall]
= [Heat transfer from the inner surface to the outer surface of west wall]

$$\alpha'_W A_W I_W(t) + h_{VW} A_W (T_V - T_{iW}) = h_{Kacr} A_W (T_{iW} - T_{oW}) \tag{14}$$

Energy balance for outer west wall surface:

[Heat transfer from the inner surface to the outer surface of west wall]
= [Heat loss to ambient by the outer west wall]

$$h_{Kacr} A_W (T_{iW} - T_{oW}) = h_o A_W (T_{oW} - T_a) \tag{15}$$

Energy balance for inner east glass cover surface:

[Heat absorbed from radiation]
+ [Heat transfer from vapor to the inner east glass cover surface]
= [Heat transfer from the inner surface to the outer surface of east glass cover]

$$\alpha'_g A_{Eg} I_{Eg}(t) + h_{VEg} A_{Eg} (T_V - T_{iEg}) = h_{Kg} A_{Eg} (T_{iEg} - T_{oEg}) \tag{16}$$

Energy balance for outer east glass cover surface:

[Heat transfer from the inner surface to the outer surface of east glass cover]
= [Heat loss to ambient by the outer east glass cover]

$$h_{Kg} A_{Eg} (T_{iEg} - T_{oEg}) = h_o A_{Eg} (T_{oEg} - T_a) \tag{17}$$

Energy balance for inner west glass cover surface:

[Heat absorbed from radiation]
+ [Heat transfer from vapor to the inner west glass cover surface]
= [Heat transfer from the inner surface to the outer surface of west glass cover]

$$\alpha'_g A_{Wg} I_{Wg}(t) + h_{VWg} A_{Wg} (T_V - T_{iWg}) = h_{Kg} A_{Wg} (T_{iWg} - T_{oWg}) \tag{18}$$

Energy balance for outer west glass cover surface:

[Heat transfer from the inner surface to the outer surface of west glass cover]
= [Heat loss to ambient by the outer west glass cover]

$$h_{Kg} A_{Wg} (T_{iWg} - T_{oWg}) = h_o A_{Wg} (T_{oWg} - T_a) \tag{19}$$

Energy balance for vapor:

[Heat transfer from water to vapor] + [Heat transfer to vapor from the inner north wall]
+ [Heat transfer to vapor from the east side strap layer of water-wick]
+ [Heat transfer to vapor from the west side strap layer of water-wick]
= [Heat transfer from vapor to the inner south wall]
+ [Heat transfer from vapor to the inner east wall]
+ [Heat transfer from vapor to the inner west wall]
+ [Heat transfer from vapor to the inner east glass cover surface]
+ [Heat transfer from vapor to the inner west glass cover surface]

$$\begin{aligned} & h_{wV} A_b (T_w - T_V) + h_{NV} A_N (T_{iN} - T_V) + h_{w-wick(E)} A_{wick(E)} (T_{w-wick(E)} - T_V) \\ & + h_{w-wick(W)} A_{wick(W)} (T_{w-wick(W)} - T_V) \\ & = h_{VS} A_S (T_V - T_{iS}) + h_{VE} A_E (T_V - T_{iE}) + h_{VW} A_W (T_V - T_{iW}) + h_{VEg} A_{Eg} (T_V - T_{iEg}) + h_{VWg} A_{Wg} (T_V - T_{iWg}) \end{aligned} \tag{20}$$

Energy balance for water:

$$[\text{Heat absorbed from radiation}] + [\text{Heat transfer to water by basin}] = [\text{Heat stored in the water}] + [\text{Heat transfer to vapor from water}] + [\text{Heat loss to ambient by water}]$$

$$(1-\beta)[\alpha'_{wg}A_b\{I_{Eg}(t)+I_{Wg}(t)\}+\alpha'_{wacr}A_b\{I_E(t)+I_W(t)+I_S(t)\}] + h_{bw}A_b(T_b-T_w) = (MC)_w\frac{dT_w}{dt} + h_{wV}A_b(T_w-T_V) + h_sA_s(T_w-T_a) \quad (21)$$

Energy balance for basin:

$$[\text{Heat absorbed from radiation}] = [\text{Heat transfer to water by basin}] + [\text{Heat loss to ambient by basin}] \quad (1-\beta)[\alpha'_{bg}A_b\{I_{Eg}(t)+I_{Wg}(t)\}+\alpha'_{bacr}A_b\{I_E(t)+I_W(t)+I_S(t)\}] = h_{bw}A_b(T_b-T_w) + h_{ba}A_b(T_b-T_a) \quad (22)$$

Energy balance for wick on east side:

$$[\text{Heat absorbed from radiation}] = [\text{Heat transfer to vapor from the east side strap layer of water-wick}] \quad \beta\alpha'_{w-wick}A_{wick(E)}I_{Eg}(t) = h_{w-wick(E)}A_{wick(E)}(T_{w-wick(E)}-T_V) \quad (23)$$

Energy balance for wick on west side:

$$[\text{Heat absorbed from radiation}] = [\text{Heat transfer to vapor from the west side strap layer of water-wick}] \quad \beta\alpha'_{w-wick}A_{wick(W)}I_{Wg}(t) = h_{w-wick(W)}A_{wick(W)}(T_{w-wick(W)}-T_V) \quad (24)$$

Solving the energy balance equations of different components of the solar still (Eqs. (8)–(24)), the following differential equation of first order has been obtained:

$$\frac{dT_w}{dt} + aT_w = f(t) \quad (25)$$

The following assumptions have been made for solving Eq. (25):

(a) Time period dt ($0 < t < dt$) for approximation is small.
(b) The function $f(t)$ is constant, i.e. $f(t) = \overline{f(t)}$ for small period dt.
(c) 'a' is constant during the time period.
(d) Internal heat transfer coefficients value are determined by considering the initial value of water and condensing glass cover temperatures.

Eq. (25) has been solved to get following expression of T_w as

$$T_w = \frac{\overline{f(t)}}{a}(1-e^{-at}) + T_{w0}e^{-at} \quad (26)$$

where, T_{w0} is the temperature of basin water at $t = 0$.

$$a = \frac{\frac{h_{bw}A_bh_{ba}}{h_{bw}+h_{ba}} + h_{wV}A_b - \frac{h_{wV}A_b}{A_2} + h_sA_s}{(MC)_w} \quad (27)$$

and

$$f(t) = \frac{\left(\alpha_1 + \frac{h_{bw}A_b\alpha_2}{h_{bw}+h_{ba}} - \frac{h_{wV}A_bA_1}{A_2}\right) + \left(\frac{h_{bw}A_bh_{ba}}{h_{bw}+h_{ba}} + h_sA_s\right)T_a}{(MC)_w} \quad (28)$$

The design parameters for the solar still used in computation is given in Table 1.

The hourly yield retrieved from south wall and glass covers of the solar still can be calculated as follows:

$$\dot{M}_{eS} = \frac{h_{w-wick(avg.)}(T_{w-wick(avg.)} - T_{iS})3600}{L_{vap}} \quad (29)$$

where, L_{vap} can be calculated as follows [60,61]:

$$L_{vap} = 3.1615\times10^6\times[1-(7.616\times10^{-4}\times T_V)] \text{ for } T_V > 70^\circ\text{C}$$

and

$$L_{vap} = 2.4935\times10^6\times\begin{bmatrix}1-(9.4779\times10^{-4}\times T_V)\\+(1.3132\times10^{-7}\times T_V^2)\\-(4.7974\times10^{-9}\times T_V^3)\end{bmatrix} \text{ for } T_V < 70^\circ\text{C}$$

For the calculation of yield retrieved from south wall, the average value of wick (strap layer of water–wick spread on east and west side) temperature ($T_{w-wick(avg.)}$) and heat transfer coefficient ($h_{w-wick(avg.)}$) has been used. This is due to yield was obtained through trough (which was stick to the south wall), whose one end was located on east wall and another was located on west wall.

$$\dot{M}_{eEg} = \frac{h_{w-wick(E)}(T_{w-wick(E)} - T_{iEg})3600}{L_{vap}} \quad (30)$$

$$\dot{M}_{eWg} = \frac{h_{w-wick(W)}(T_{w-wick(W)} - T_{iWg})3600}{L_{vap}} \quad (31)$$

The total hourly yield of the solar still is calculated as [57]:

$$\dot{M}_{ew} = \dot{M}_{eS} + \dot{M}_{eEg} + \dot{M}_{eWg} \quad (32)$$

The total daily yield of the solar still is given by [57]:

$$\dot{M}_{total} = \sum_{i=1}^{i=24}\dot{M}_{ew} \quad (33)$$

In the present study, the height of east (E) and west (W) walls have been taken 12 cm only. Therefore, due to space constraint, troughs on the inner location of the east and west walls for distillate collection have not been provided [57].

The instantaneous thermal energy efficiency of the solar still can be expressed as equation given by [57]:

$$\eta_i = \frac{\dot{M}_{ew}\times L_{vap}}{I(t)_{input}\times3600}\times100 \quad (34)$$

where, $I(t)_{input}$ is the total input solar energy (instantaneous) to the solar

Table 1
Design parameters used in computation for the solar still.

Parameters	Values	Parameters	Values
A_N	0.50 m^2	l_g	0.004 m
A_b	2.0 m^2	l_{acr}	0.003 m
A_S	0.50 m^2	M_w	40 kg
A_E	0.12 m^2	σ	5.67 × 10^{-8} W/m^2–K^4
A_W	0.12 m^2	t	3600 s
A_{Eg}	1.06 m^2	α_g	0.05
A_{Wg}	1.06 m^2	α_b	0.7
$A_{wick(E)}$	0.808 m^2	α_w	0.1
$A_{wick(W)}$	0.808 m^2	α_{acr}	0.04
ρ_w	1000 kg/m^3	α_{FRP}	0.90
C_w	4187 J/kg –K	β	0.728
h_{bw}	100 W/m^2–K	ε_{acr}	0.94
h_s	5.321 W/m^2–K	ε_{FRP}	0.745
k_b, k_{FRP}	0.351 W/m–K	ε_w, ε_g	0.9
k_g	0.780 W/m–K	R_g	0.05
k_{acr}	0.2 W/m–K	R_w	0.05
l_b, l_{FRP}	0.005 m	R_{acr}	0.04

$\alpha'_{acr} = (1-R_{acr})\alpha_{acr}$

still and given by the following equation [57]:

$$I(t)_{input} = I_{Eg}(t) \times A_{Eg} + I_{Wg}(t) \times A_{Wg} + I_E(t) \times A_E + I_W(t) \times A_W + I_S(t) \times A_S \tag{35}$$

4. Heat transfer coefficients

The internal heat transfer is accountable for the carrying of water (pure or potable water) in vapor form suspends all the uncleanliness in the basin, whereas, the external heat transfer through transparent walls and condensing glass covers are accountable for the condensation of water vapor as distillate. The internal heat transfer occurs within the solar distiller, which mainly consists of evaporation, convection and radiation. The external heat transfer is mainly accomplished by conduction, convection and radiation processes, which are independent of each other [61].

4.1. Internal heat transfer coefficient

It is previously said in this study, a hypothetical vapor surface is considered for all the heat interactions to the surrounding surface(s). For calculating the internal convective and evaporative heat transfer coefficients, the generalized Dunkle and Cooper–Dunkle's model have been used for find out the respective heat transfer coefficients.

Convective heat transfer coefficient is given as [36,38,60,61]:

$$h_{conv} = 0.884\left[(T_V - T_{insurf}) + \frac{(P_V - P_{insurf})(T_V + 273)}{(268.9 \times 10^3 - P_V)}\right]^{1/3} \tag{36}$$

Evaporative heat transfer coefficient is given as [36,38,60,61]:

$$h_{evap} = (0.016273)h_{conv}\left(\frac{P_V - P_{insurf}}{T_V - T_{insurf}}\right) \tag{37}$$

Internal radiative heat transfer coefficient is given as [36,60,61]:

$$h_{rad} = \varepsilon_{eff}\sigma[(T_V + 273)^2 + (T_{insurf} + 273)^2][T_V + T_{insurf} + 546] \tag{38}$$

where, ε_{eff} can be calculated as follows [36,38,60,61]:

$$\varepsilon_{eff} = \left(\frac{1}{\varepsilon_V} + \frac{1}{\varepsilon_{insurf}} - 1\right)^{-1} \tag{39}$$

where, T_{insurf} indicates the inside surface i.e. east; west; and south walls, east and west glass covers of the solar still.

In multi–wick solar still, one can assume that, wick is only responsible for evaporation and hence, for calculating the coefficient of heat transfer for wick (east and west side wick), only evaporative heat transfer coefficient is measured and given as:

$$h_{w-wick(E)} = (0.016273)h_{conv,w-wick(E)}\left(\frac{P_{w-wick(E)} - P_V}{T_{w-wick(E)} - T_V}\right)\text{(for East side)} \tag{40}$$

and

$$h_{w-wick(W)} = (0.016273)h_{conv,w-wick(W)}\left(\frac{P_{w-wick(W)} - P_V}{T_{w-wick(W)} - T_V}\right)\text{(for west side)} \tag{41}$$

where, $h_{conv,\ w-wick}$ is calculated on East and West side as:

$$h_{conv,w-wick} = 0.884\left[(T_{w-wick} - T_V) + \frac{(P_{w-wick} - P_V)(T_{w-wick} + 273)}{(268.9 \times 10^3 - P_{w-wick})}\right]^{1/3} \tag{42}$$

The total internal heat transfer coefficient for walls of the solar still are summation of internal convective and radiative heat transfer coefficient and given as:

For example, h_{VS} is coefficient of total internal heat transfer from south wall to vapor in W/m^2–K.

$$h_{VS} = h_{VS,conv} + h_{VS,rad} \tag{43}$$

$$h_{VS} = 0.884\left[(T_V - T_{iS}) + \frac{(P_V - P_{iS})(T_V + 273)}{(268.9 \times 10^3 - P_V)}\right]^{1/3} + \varepsilon_{eff}\sigma[(T_V + 273)^2 + (T_{iS} + 273)^2][T_V + T_{iS} + 546] \tag{44}$$

4.2. External heat transfer coefficient

The heat transfer from the distiller unit to the atmosphere is called as external heat transfer. It is categorized in two types: (i) the heat transfer from the condensing glass cover to the ambient, which is known as top heat loss and (ii) the heat transfer from the sides of insulation and bottom (basin) to the ambient, which is known as bottom and side loss [38,61].

Heat transfer from condensing glass cover surface to ambient air is attributed to convection and radiation. The total (combined) convective and radiative heat transfer coefficient from glass cover surface to ambient is given as [61,62]:

$$h_o = 5.7 + 3.8v \tag{45}$$

The heat transfer from basin to ambient atmosphere takes place by conduction through the basin then combined convection and radiation. The heat transfer coefficient from basin to ambient is given as [62]:

$$h_{ba} = \left[\frac{1}{h_b} + \frac{1}{h_o}\right]^{-1} \tag{46}$$

where, h_b is given as [62]:

$$h_b = \frac{k_b}{l_b} \tag{47}$$

All the unknowns in above equations and heat transfer coefficients used in thermal modeling are given in Appendix A.

5. Exergy analysis

The performance evaluation of multi–wick solar still, which is a sustainable conversion system based on renewable energy, rooted by the first law of thermodynamics i.e. energy analysis, which only considering the energies entering and exiting through the system. However, the methodology opt for tracking all aspects of energy exploitation or utilization in the elements of a thermal system or processes by energy analysis is alone not sufficient. Hence, a qualitative tool, which analyzes the system processes more comprehensively is represented by exergy analysis [63]. Exergy analysis is based on the second law of thermodynamics and analyzing the irreversibility rate or destruction in the components of thermal systems. So, the use of exergy analysis is recommended to measure the performance of any solar energy applications [63]. It is found in the literature that, the recent studies has been carried out for the solar driven desalination applications where exergy analysis is used as an efficient tool to improve the overall efficiency, design aspects, identify the system inefficiencies, and performance evaluation [1,59,63].

In most of the solar–driven desalination techniques, the second law of thermodynamics and Petela exergy's equation for the solar radiation is the basic principle for the exergy analysis. The Petela expression is given as [64]:

$$Ex_{sun} = I(t)_{input}\left[1 + \frac{1}{3}\left(\frac{T_a}{T_{sun}}\right)^4 - \frac{4}{3}\left(\frac{T_a}{T_{sun}}\right)\right] \tag{48}$$

where, T_a is the ambient temperature (in Kelvin) and T_{sun} is the sun temperature (in Kelvin) and T_{sun}value is approximated as 6000 K.

The hourly exergy output of the solar still is the exergy of useful heat indulge in the production of distillate yield through the evaporation–condensation process and given by the following equation [65]:

$$Ex_{output} = \frac{\dot{m}_{ew} L_{vap}}{3600}\left(1 - \left[\frac{(T_a + 273)}{(T_{w-wick} + 273)}\right]\right) \tag{49}$$

The instantaneous exergy efficiency of the solar still is determined as the ratio of exergy output or gain associated with the yield to the total input exergy (solar radiation exergy).

Instantaneous exergy efficiency can be given as [65]:

$$\eta_{ex,ins} = \frac{\frac{\dot{m}_{ew} L_{vap}}{3600}\left(1 - \left[\frac{(T_a + 273)}{(T_{w-wick} + 273)}\right]\right)}{I(t)_{input}\left(1 + \frac{1}{3}\left[\frac{(T_a + 273)}{(T_{sun} + 273)}\right]^4 - \frac{4}{3}\left[\frac{(T_a + 273)}{(T_{sun} + 273)}\right]\right)} \tag{50}$$

The monthly variation of exergy and annual exergy output (or gain) for the solar still with jute and black cotton wicks at 1 cm and 2 cm water depth have been evaluated and presented in Table 2.

6. Instrumentation and uncertainty analysis

A digital temperature scanner or indicator (least count: 0.1 °C) with 10–channel and holding switch was used with calibrated type T Copper–Constantan thermocouples (range: –40-350 °C) to measure the temperature of different components or locations inside the solar still. Thermocouples has been placed at the basin, inside and outside surface of glass cover and walls. Two thermocouples has been placed at the gap between the water/wick surface and inner glass cover (one in the gap between inner glass cover–wick surface, and another in the gap between wick surface–water surface) to measure the air–vapor mixture's temperature. The wick's temperature was measured by placing a thermocouple at each side water–wick layer. An infrared thermometer (model: FLUKE 62 max; range: –30-500 °C; least count: 0.1 °C) was used to measure the outside temperature of different locations in the solar still. A mercury–in–glass thermometer (range: –10-110 °C; least count: 1 °C) was used to measure the water temperature, vapor temperature, and ambient temperature. A solarimeter or solar power meter (model: AMPROBE SOLAR–100; range: 0–1999 W/m^2; least count: 0.1 W/m^2) was used to measure the intensity of solar radiation. A digital anemometer (model: FLUKE BTH401; least count: 0.1 °C and 0.1 m/s) was used to measure the wind speed and ambient temperature. A scaled cylindrical container (least count: 2 ml) was used to measure the distillate collection.

Uncertainties in measurement during experimentation can be evaluated as reported by Akpinar [66]. Using the values of uncertainty in measuring instruments given in Table 3, the total uncertainties in temperature, solar radiation, wind velocity and yield measurement has been found to be 0.22, 1.4, 0.14 and 2.23, respectively. The total uncertainty in experimental measurement has been found to be ± 2.64. Therefore, it is observed that all uncertainties during experimentation were in the expectable limit. Statistical tools given by Chapra and Canale [67] have been used to evaluate the correlation coefficient (r–value) and root mean square percentage deviation (e–value). Procedure for calculating the r–value and e–value are given in Appendix A.

Table 2
Annual exergy output of the solar still with jute and black cotton wicks at 1 cm and 2 cm water depth in each month in Allahabad (U.P.), India.

Month	Exergy output (kWh) at 1 cm water depth		Exergy output (kWh) at 2 cm water depth	
	Jute wick	Black cotton wick	Jute wick	Black cotton wick
August 2015	6.05	7.92	5.77	7.12
September 2015	7.46	8.76	6.19	7.62
October 2015	5.36	6.54	4.71	5.92
November 2015	4.77	6.39	3.61	5.25
December 2015	2.50	3.18	2.34	2.95
January 2016	1.73	2.87	1.21	2.49
February 2016	2.76	4.12	2.05	3.24
March 2016	10.08	12.15	9.89	10.20
April 2016	10.15	12.34	10.02	10.22
May 2016	10.85	13.78	10.16	11.23
June 2016	10.37	12.43	9.78	11.38
July 2016	4.18	6.88	3.56	4.45
Annual exergy output $E_{ex,ann}$(kWh)	76.26	97.36	69.29	82.07

Table 3
Uncertainty in measuring instruments.

Measuring instruments	Uncertainty value
Connection point	$W_{connection\ point} = \pm 0.1$
Digital anemometer	$W_{anemometer} = \pm 0.1$
Infrared thermometer	$W_{ir\ thermometer} = \pm 0.1$
Reading error	$W_{readings} = \pm 0.1$
Scaled cylindrical container	$W_{cylindrical\ container} = \pm 2$
Solarimeter	$W_{solarimeter} = \pm 1$
Thermocouple	$W_{thermocouple} = \pm 0.1$
Thermometer	$W_{thermometer} = \pm 0.1$

7. Methodology

Based on the basic energy balance equations of the solar still, a software–code have been developed in MATLAB 2015a to evaluate the water temperature. The numerical calculations have been performed for a typical day under the climatic condition of Allahabad, India.

Following procedure or steps have been taken for the analysis of the solar still system:

(a) Hourly variation of solar radiation, vapor temperature, ambient temperature and wind velocity data have been taken experimentally.
(b) Different values of internal, external, overall, and conductive heat transfer coefficients have been evaluated.
(c) A numerical calculation for water temperature (Eq. (25)) has been done in terms of constants (Eq. (27)) and (Eq. (28)), which is further solved for time interval dt and finally gives the expression for water temperature (Eq. (26)). (Initial value of water temperature has been used to found out the theoretical value of water temperature)
(d) With the help of water temperature, solar still's wall temperature; glass cover temperature; and wick (strap layer of water–wick) temperature have been evaluated.
(e) The theoretical temperature values obtained from thermal modeling have been validated by experimental data.
(f) After estimating the values of annual energy; annual exergy; and productivity (yield), the energy matrices, environmental cost, and exergoeconomic parameter has been evaluated.

8. Energy matrices

In the energy analysis, energy payback time (EPBT), life cycle conversion efficiency (LCCE), and energy production factor (EPF) have been evaluated to extract the performance of the modified multi–wick solar still and hence it is requisite to evaluate these energy parameters for any sustainable technology which is reliable on solar energy. For any renewable energy based technology or system, the energy evolved by the system during its whole life must be greater than the energy harnessed by it during manufacturing [40,59].

8.1. Energy payback time (EPBT)

Energy payback time of the solar still defines the time duration

Table 4
Embodied energy of different components of the solar still with jute and black cotton cloths.

Name of component	Mass of component (kg)	Energy density (MJ/kg)	Embodied energy in MJ	Embodied energy in kWh
FRP body	23.32	92.30	2152.44	598
Acrylic body	3.54	100	354	98.34
Glass cover	19.94	15.90	317.12	88
GI iron stand	8.0	49.968	399.74	111.04
Outlet nozzle	0.10	44.10	4.41	1.22
Black paint	0.50	90.40	45.20	12.55
Silicon rubber gaskets	2.13	11.83	25.19	6.99
Glass putty	2.50	5.30	13.25	3.68
Concrete block	52.80	0.94	49.63	13.78
Jute cloth	5.0	55	275	76.39
Black cotton cloth	2.50	143	357.5	99.30
Total embodied energy (with jute cloth)			3635.98	1009.99
Total embodied energy (with black cotton cloth)			3718.48	1032.91

expected to recover the total energy fatigued in the material preparation for the system and its components construction. In general, the EPBT depends on the embodied energy and the annual energy yield i.e. distillate output obtained from modified multi–wick solar still. For the estimation of the embodied energy of various components of the solar still, one can essentially require the information about the energy densities of different material used in the fabrication of solar still. The embodied energy of different components of the solar still with jute and black cotton cloths is presented in Table 4. On the basis of energy and exergy, EPBT can be evaluated as [40,59,68]:

$$(EPBT)_{en} = \frac{Embodied\ energy\ in\ (E_{in})}{Annual\ energy\ out\ (E_{out,ann})} \tag{51}$$

$$(EPBT)_{ex} = \frac{Embodied\ energy\ in\ (E_{in})}{Annual\ exergy\ out\ (E_{ex,ann})} \tag{52}$$

The value of EPBT should be kept as low as possible to build any renewable energy system cost effective.

8.2. Energy production factor (EPF)

The energy production factor (EPF) establishes the overall execution of the renewable energy system. It measures the overall performance of the modified multi–wick solar still. The EPF on the basis of energy and exergy are evaluated as [40,59,68]:

$$(EPF)_{en} = \left[\frac{Embodied\ energy\ in\ (E_{in})}{Annual\ energy\ out\ (E_{out,ann})}\right]^{-1} \tag{53}$$

$$(EPF)_{ex} = \left[\frac{Embodied\ energy\ in\ (E_{in})}{Annual\ exergy\ out\ (E_{ex,ann})}\right]^{-1} \tag{54}$$

8.3. Life cycle conversion efficiency (LCCE)

Life cycle conversion efficiency (LCCE) is the ratio of the net output from the system to the solar radiation (solar thermal energy) retrieved by the solar still over the entire life span of the system. Higher value of LCCE signifies that the system is more efficient. The life cycle conversion efficiency of the solar still can be evaluated as [40,59,68]:

$$(LCCE)_{en} = \frac{(E_{out,ann} \times n) - E_{in}}{E_{sol(en),ann} \times n} \tag{55}$$

$$(LCCE)_{ex} = \frac{(E_{ex,ann} \times n) - E_{in}}{E_{sol(ex),ann} \times n} \tag{56}$$

where, $E_{out,\ ann}$ is the annual solar energy output i.e. yield production, E_{in} is the embodied energy, $E_{sol,\ ann}$ is the annual solar energy retrieved or incident on the solar still (total input energy), $E_{ex,\ ann}$ is the annual exergy gain, and n is the life span of the solar still. The energy and exergy input and outputs for the solar still with jute and black cotton wicks at 1 cm and 2 cm water depth on annual basis is presented in Table 5.

9. Enviroeconomic analysis

An enviroeconomic analysis is focused on how efficiently one can use the renewable sources of energy with less emission of CO_2 to the environment. It is also motivating to use such sustainable technology which is based on solar energy and does not pollute the ambient environment. Enviroeconomic analysis associated with the cost of CO_2 emission and tries to mitigate the CO_2 level in the environment (CO_2 emissions as low as possible). The average carbon dioxide (CO_2) emitted amount per kWh for electricity production from the best quality of coal is approximately 0.96 kg of CO_2/kWh [40,69]. For the Indian condition, if the transmission and distribution losses are taken 40% and domestic appliances (electrical loss) is around 20%, then the amount of CO_2 emission comes out to be 2.0 kg per kWh unit of power consumption. Therefore,

The amount of CO_2 mitigated per annum (φ_{CO_2}) can be evaluated as [40,70]:

$$\text{On the basis of energy; } \varphi_{CO_2} = \frac{(\psi_{CO_2}/0.38) \times E_{out,ann}}{10^3} \tag{57}$$

$$\text{On the basis of exergy; } \varphi_{CO_2} = \frac{\psi_{CO_2} \times E_{ex,ann}}{10^3} \tag{58}$$

where, ψ_{CO_2} is the amount of CO_2 emitted per unit electricity or average CO_2 equivalent intensity for electricity production from coal (2.04 kg CO_2/kWh).

The business of carbon credits (environmental cost or environmental parameter) was created to reduce the effect of greenhouse gases (GHG) emission into the atmosphere by alleviating the carbon footprint. Therefore, the environmental cost or carbon credits earned by the solar still is given as:

$$Z_{CO_2} = \varphi_{CO_2} \times z_{CO_2} \tag{59}$$

where, z_{CO_2} is the international price of carbon (€11.09 per ton of CO_2).

10. Exergoeconomic analysis

Exergoeconomic analysis integrates the economic analysis with the exergy. Generally, it is a combination of cost analysis with the exergy analysis to carried out the overall performance improvement in the renewable energy system. It also helps the engineers or scientists to

Table 5
Annual energy and exergy input, and gain obtained for the solar still with jute and black cotton wicks at 1 cm and 2 cm water depth in Allahabad (U.P.), India.

Particulars	Energy and exergy on annual basis (kWh) at 1 cm water depth		Energy and exergy on annual basis (kWh) at 2 cm water depth	
	Jute wick	Black cotton wick	Jute wick	Black cotton wick
Energy output (E_{out})	1457.61	1620.16	1346.88	1478.79
Solar energy input ($E_{sol(en)}$)	5625.97	5698.72	5681.97	5760.52
Exergy output (E_{ex})	76.26	97.36	69.29	82.07
Exergy input ($E_{sol(ex)}$)	5242.78	5311.99	5297.01	5368.53

look out an alternative or suggestive ways to ameliorate the renewable energy based system's performance from the cost approach.

The exergoeconomic parameter based on exergy for the solar still can be calculated as [40,71]:

$$R_{ex} = \frac{E_{ex,ann}}{UAC} \tag{60}$$

where, $E_{ex,\ ann}$ is the annual exergy gain and UAC is the uniform annual cost of the solar still.

The generalized expressions of uniform annual cost (*UAC*), net present value (*NPV*), sink fund factor (*SFF*), and capital recovery factor (*CRF*) are calculated given below:

$$UAC = (NPV \times CRF) + (M_s \times CRF) - (SV \times SFF) \tag{61}$$

The net present value (*NPV*) for the 30 years of life span of solar distiller is given by Agrawal and Tiwari [71].

$$NPV = P + R_1 \times \left[\frac{(1+i)^n - 1}{i(1+i)^n}\right]_{i,n} + P_{wick\,(10,1)} \times \left[\frac{1}{(1+i)^n}\right]_{i,10} + P_{wick\,(20,2)} \times \left[\frac{1}{(1+i)^n}\right]_{i,20} + P_{wick\,(30,3)} \times \left[\frac{1}{(1+i)^n}\right]_{i,30} - SV \times \left[\frac{1}{(1+i)^n}\right]_{i,n} \tag{62}$$

Similarly, net present value (*NPV*) for the 40 years of life span of solar distiller is calculated as [71]:

$$NPV = P + R_1 \times \left[\frac{(1+i)^n - 1}{i(1+i)^n}\right]_{i,n} + P_{wick\,(10,1)} \times \left[\frac{1}{(1+i)^n}\right]_{i,10} + P_{wick\,(20,2)} \times \left[\frac{1}{(1+i)^n}\right]_{i,20} + P_{wick\,(30,3)} \times \left[\frac{1}{(1+i)^n}\right]_{i,30} + P_{wick\,(40,4)} \times \left[\frac{1}{(1+i)^n}\right]_{i,40} - SV \times \left[\frac{1}{(1+i)^n}\right]_{i,n} \tag{63}$$

In a similar way, the net present value (NPV) for 50 years of life time of solar still can be evaluated.

$$CRF = \frac{i \times (1+i)^n}{(1+i)^n - 1} \tag{64}$$

$$SFF = \frac{i}{(1+i)^n - 1} \tag{65}$$

where, *P* is the present or capital cost, *SV* is the salvage value, R_1 is the operational cost, M_s is the maintenance cost, *n* is the life span of solar still and $P_{w(10,1)}$, $P_{w(20,2)}$, $P_{w(30,3)}$, $P_{w(40,4)}$ be the wick replacement cost in every 10 years. The total cost of the solar still after manufacturing was taken as present or capital cost. The salvage value (*SV*) and maintenance cost (M_s) were taken to be 15% and 10% of the capital cost, respectively [57,59]. The operational cost of the solar still was taken to be Rs. 500 per year, which includes regular cleaning of glass cover, walls, and leakage check. Overall, operational cost associated with the activities pertaining to run the solar still whereas maintenance keep it working (or proper functioning). The wick replacement cost was taken to be Rs. 400 in every 10 years. The total fabrication cost and cost of different components of the solar still are given in Table 6.

11. Results and discussion

In this section, the data observed from the experiments and results obtained from the theoretical modeling of the solar still has been discussed for the climatic condition of Allahabad (U.P.), India. Energy matrices (EPBT, EPF, and LCCE), annual exergy, enviroeconomic; and exergoeconomic analysis has been presented for 365 days in a year. A brief analysis has also been carried out for 300 days in a similar manner excluding the rainy and fully cloudy days. The data collected from the experimental work and relevant equations have been put into MATLAB 2015a computation program in order to validate the theoretical results. The EXCEL (Microsoft Excel 2013) program have also been used to compute the exergy output, embodied energy, energy matrices, environmental and exergoeconomic parameters.

Table 6
Cost of the components associated with the solar still.

Components	Cost[a] (*Rs.*)	Cost[a] (US$)
FRP body @400/kg	9328	143.81
Acrylic body @182.50/kg	646	9.96
Glass cover (1.06 m^2)	1100	16.96
Iron stand	560	8.63
Inlet/Outlet nozzle	70	1.08
Silicon gaskets	360	5.55
Black paint and glass putty	160	2.46
Labor and other charges	1500	23.12
Jute cloth (for jute wick)	276	4.25
Cotton cloth (for cotton wick)	438	6.75
Total cost of the still (with jute wick)	14,000	215.82
Total cost of the still (with black cotton wick)	14,162	218.32

[a] 1 US$ = Indian Rs. 64.86 on 16/03/2018, (costs are based on Allahabad (U.P.) market rate).

Fig. 4 shows the hourly variation of global solar radiation; diffuse radiation (W/m^2), and ambient temperature (°C) during the experimental periods with respect to time (h) for a typical day in the month of March 2016. It has been observed that the global solar radiation increases till 11:00 h and then decreases till the evening hours (end of sunshine). The maximum measured value was found to be 1148 W/m^2 at 11:00 h. The ratio of diffuse radiation to global solar radiation has been found to be 0.237 (or 23.7%), which clearly shows that the weather condition for the typical day was ‘clear or blue sky’ condition and the sunshine hour was observed between 10 h–11 h [72]. The amount of solar radiation retrieved by the solar still was higher in the time period between 10:00–14:00 h. In this time duration, the variation in the incident solar radiation's intensity was low and remain neighbored to the average intensity of solar radiation of this period [57,62]. The maximum ambient temperature during the day of experiment was observed to be 37 °C at 11:00 h. The average ambient temperature was found to be 28.34 °C.

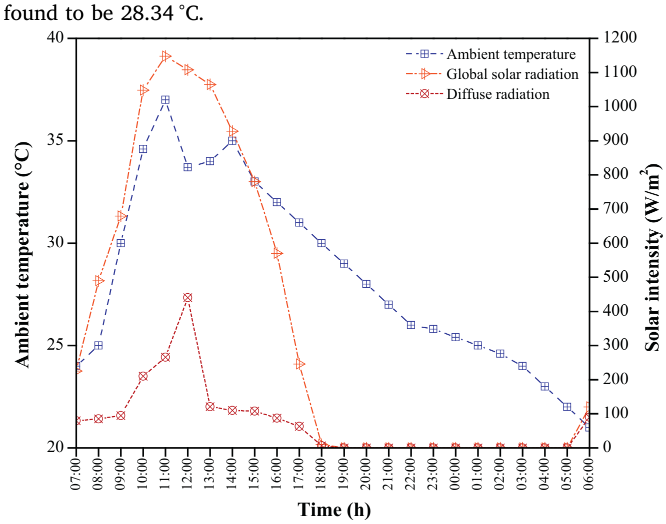

Fig. 4. Hourly variation of global solar radiation, diffuse radiation, and ambient temperature during experimentation for a typical day in the month of March 2016.

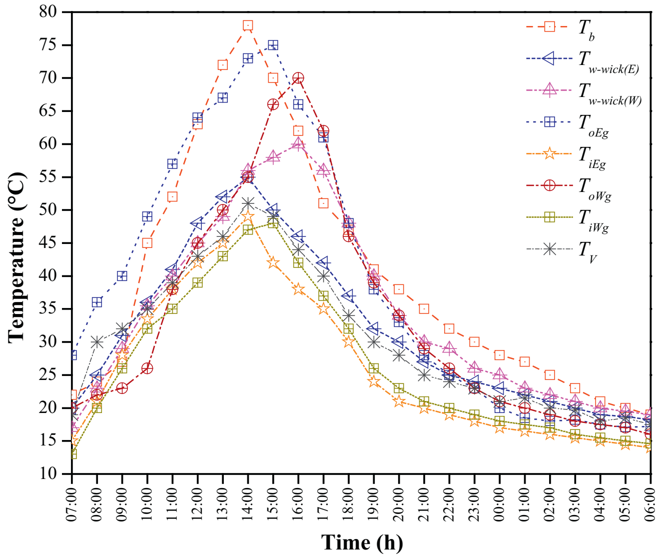

Fig. 5. Hourly variation of basin, vapor, east and west wicks, east and west glass covers temperature during experimentation for a typical day in the month of March 2016.

Fig. 5 shows the hourly variation of basin temperature, vapor temperature, east and west side wick temperature, inside and outside east and west glass covers temperature (°C) during the experimental periods with respect to time (h) for a typical day in the month of March 2016. The maximum basin; vapor; east wick; west wick; outer east glass; inner east glass; outer west glass; and inner west glass temperatures were observed to be 78 °C at 14:00 h; 51 °C at 14:00 h; 55 °C at 14:00 h; 60 °C at 16:00 h; 75 °C at 15:00 h; 49 °C at 14:00 h; 70 °C at 16:00 h; and 48 °C at 15:00 h, respectively. It has been observed from the figure that the inner east and west glass temperatures were lower than the respective east and west side wetted cloth temperatures, this is attributed to the reduced heat capacity of water in the thin film of both side wicks. The similar behavior has been obtained in the study of Sharon et al. [73]. The average temperature variation between east wick– inside east glass cover and west wick–inside west glass cover were found to be 5.66 °C and 7.85 °C, respectively.

Fig. 6 shows the hourly variation of theoretical and experimental water temperature (°C) with respect to time (h) for a typical day in the month of March 2016. The theoretical water temperature was found to be higher than the experimental water temperature during morning hours (till 11:00 h), where water gains the maximum theoretical value of 52 °C at 11:00 h. After 11:00 h, theoretical water temperature decreases while the experimental water temperature was higher than the theoretical value up to 20:00 h. The maximum experimental water temperature was observed to be 57 °C at 14:00 h. The maximum deviation between the experimental and theoretical water temperature was found to be 8 °C observed around 14:00 h. The r-value and e-value have been shown in the figure. The coefficient of correlation and root mean square percent deviation values were found to be 0.964 and 9.94%, respectively. So, one can be observed that there is close agreement between the experimental and theoretical values of water temperature.

Fig. 7 shows the hourly variation of theoretical and experimental average temperature of east and west side spread strap layer of water–wick (°C) with respect to time (h) for a typical day in the month of March 2016. It has been observed that the temperature profiles of both the experimental and theoretical average temperature of strap layer of water–wick is nearly same. The temperatures of both profiles were found to increase linearly as radiation starts to incident on the solar still achieved the maximum value around 14:00 h and then start to decrease during evening hours. The maximum experimental and theoretical average temperature of strap layer of water–wick was found to be 55.5 °C at 14:00 h and 60.04 °C at 14:00 h, respectively. The maximum temperature difference between the average experimental and theoretical value was found to be 7.65 °C observed around 11:00 h. The coefficient of correlation (r-value) and root mean square percent deviation (e-value) were found to be 0.991 and 9.84%, respectively. Both temperatures profile shown the similar trend and having the fair agreement between each other.

Fig. 8 shows the hourly variation of theoretical and experimental yields (ml) with respect to time (h) for a typical day in the month of March 2016. The depth of water in the basin was 2 cm during the day of experimentation. It has been observed that both the curves follow the same trends as yields increases gradually to a maximum value during noon and then decline during evening periods. The maximum experimental and theoretical yield were observed to be 1043 ml/h (0.52 l/m^2 h) at 13:00 h and 1078 ml/h (0.53 l/m^2 h) at 15:00 h, respectively. It was also seen that during the morning (up to 10:00 h) and night (after 21:00 h) periods, the experimental and theoretical values were closer to

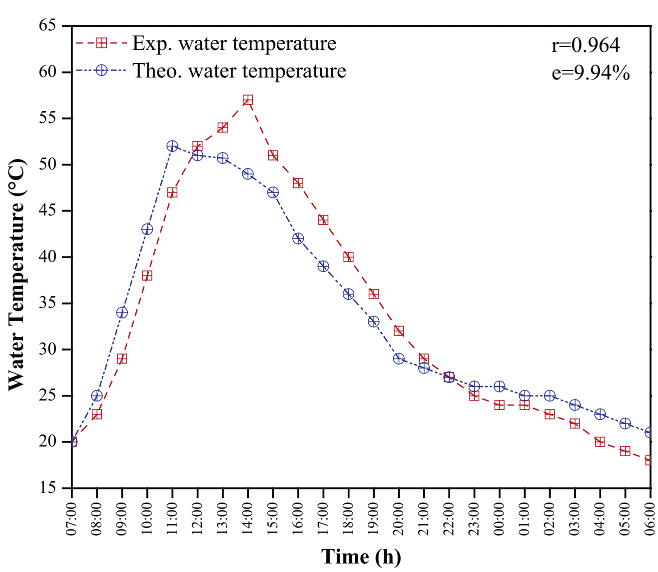

Fig. 6. Hourly variation of experimental and theoretical water temperature for a typical day in the month of March 2016.

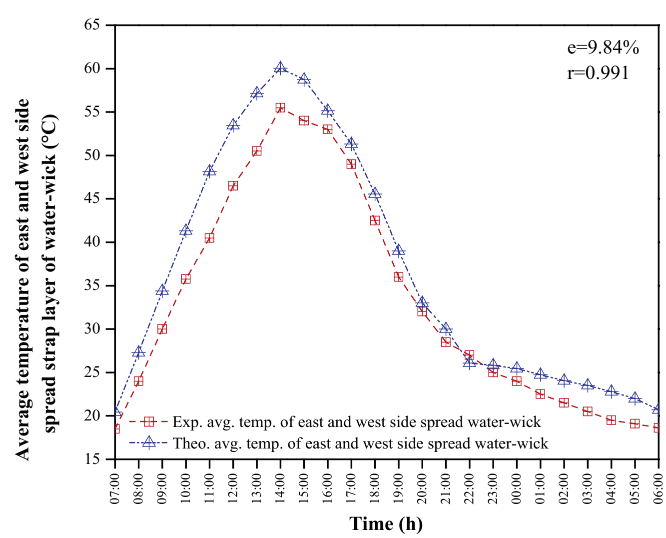

Fig. 7. Hourly variation of experimental and theoretical average temperature of east and west side spread wick (strap layer of water–wick) for a typical day in the month of March 2016.

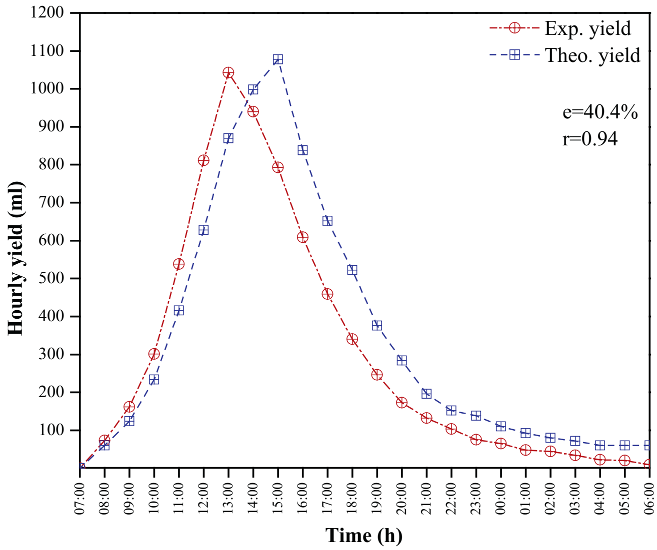

Fig. 8. Hourly variation of experimental and theoretical yield for a typical day in the month of March 2016.

each other, this is mainly due to reduced heat storage capacity of wetted wicks which can be further justified by reduced yield productivity during night–time (nocturnal yield). The experimental and theoretical nocturnal yield production was observed to be 962 ml/day and 1620 ml/day, respectively, which occupies only 13.67% and 20% of the total yield, respectively. The coefficient of correlation and root mean square percent deviation values were found to be 0.94 and 40.4%, respectively. The higher e-value has been found due to very low yield output during the night–time (nocturnal yield). It has been noticed from the Fig. 4 that the maximum intensity of global solar radiation retrieved by the solar still was observed at 11:00 h, but the maximum yield obtained at 13:00 h. This is attributed to the heat storage effect of water accumulated in the basin and time delay between the evaporation–condensation processes. It can be observed that the experimental and theoretical yield curves has been shown the closer agreement, which validates the present thermal (or thermodynamic) modeling used for the solar still.

Fig. 9 shows the experimental and theoretical cumulative yield (ml/day) with respect to time (h) for a typical day in the month of March 2016. The experimental and theoretical cumulative yield production was found to be 7040 ml/day (3.52 l/m^2 day) and 8101 (4.05 l/m^2 day), respectively. The cumulative experimental yield for the solar still was lower than the theoretical value by 15.07%. The deviations in the measured and theoretical values might be due to the using approximate heat transfer coefficient models, loss of condensate due to falling of droplets into feed water before reaching to the troughs, trapping of very few amount of distillate in troughs and evaporation of condensate during the collection process, limitations evolved due to assumption during modeling, and uncertainties in real time climatic condition of location.

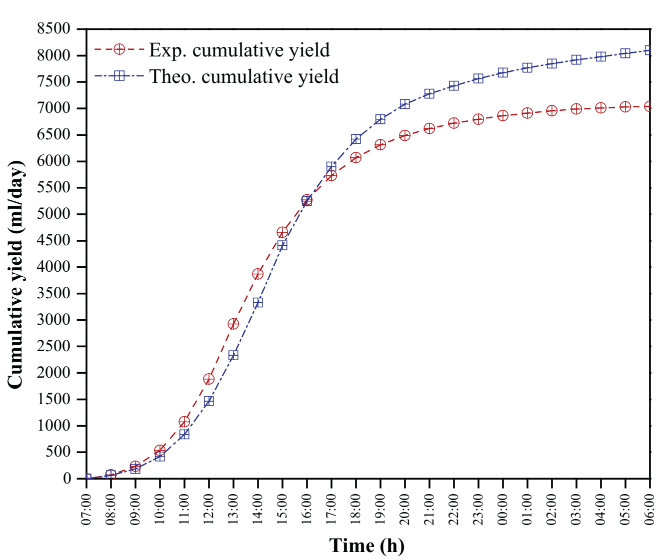

Fig. 9. Hourly experimental and theoretical cumulative yield for a typical day in the month of March 2016.

Fig. 10 shows the hourly variation of instantaneous energy efficiency (η_{i-th}) and instantaneous exergy efficiency, η_{i-ex} (%) with respect to time (h) for a typical day in the month of March 2016. It has been observed that the thermal efficiency has been increased during 09:00 h–14:00 h. In the morning hours up to 10:00 h, though sufficient amount of yield has been gained but due to considerable enhancement in the solar radiation intensity, the gain in thermal efficiency was lesser. After 10:00 h, there was a significant increase in the thermal efficiency due to higher yield and water temperature values. Between 14:00 h–15:00 h, the instantaneous energy efficiency reduces due to drop in solar radiation intensity, sudden drop in water temperature; and average temperature of both side spread wicks. After 15:00 h, the thermal efficiency again rises due to sufficient amount of solar thermal energy stored by the solar still (due to transparency of east, west, and south walls) while the intensity of solar radiation still reduced, which causes evaporation–condensation processes to yielding distillate in the subsequent evening hours. Therefore, in the evening hours (up to 17:00 h), instantaneous energy efficiency increases and achieved its maximum value of 35% at 17:00 h. In the previous studies, it is said that the time duration between 09:00 h–15:00 h is more persistent to characterize the solar still for the Allahabad, (U.P.) climatic conditions in summer season [57]. The maximum value of measured instantaneous energy efficiency in time period 09:00 h–15:00 h was found to be 27.51% at 14:00 h. The overall thermal efficiency of solar still was found to be 21.52%. The theoretical instantaneous energy efficiency curve has shown the same trend up to 14:00 h, but after 14:00 h theoretical efficiency still rises while drop in measured thermal efficiency. This is due to the fact that the maximum theoretical yield was obtained at 15:00 h while energy input to solar still has been reduced. After 15:00 h, though input energy still drops, a significant amount of theoretical yield was obtained in the evening hours. So, the theoretical instantaneous energy efficiency curve has been shown the increasing behavior with respect to time. The maximum value of theoretical instantaneous energy efficiency was noticed to be 52.78% at 17:00 h. The

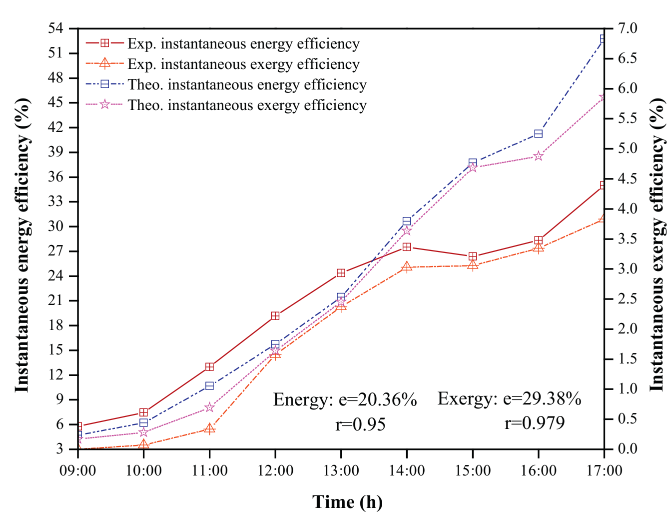

Fig. 10. Hourly variation of experimental and theoretical instantaneous energy and exergy efficiency for a typical day in the month of March 2016.

coefficient of correlation and root mean square percent deviation values were found to be 0.95 and 20.36%, respectively for instantaneous energy efficiency.

The instantaneous exergy efficiency has been found to follow the same behavior as instantaneous energy efficiency. In the exergy output and efficiency equation i.e. Eqs. (49) and (50), the temperature of water in strap layer of wick has been considered instead of water temperature which is accumulated in the basin. Since in the multi–wick solar still, water to reach up to the top strap layer of wicks through the capillary action and a thin layer of water is formed on the whole surface, the more amount of water will be available for the effective evaporation [57]. So, the exergy associated with the improved amount of distillate will be higher with a relatively low temperature of water in the wick. The instantaneous exergy efficiency increases in the time interval 09:00 h–14:00 h, but in the time period 09:00 h–11:00 h, this rise in the exergy efficiency was slower because of increase in the ambient temperature. After 11:00 h, the sharp increment in the average water (water in strap layer of both side wicks) temperature and fall in ambient temperature causes rise in the exergy efficiency. In time interval 13:00 h–14:00 h, the exergy efficiency was slightly reduced due to increment in the ambient temperature. It was noticed that in the time interval 14:00 h–15:00, instantaneous exergy efficiency was almost constant, while a significant drop in solar radiation intensity has been observed. It is mainly due to the fall in average water (water in strap layer) temperature during this time period. After 15:00 h, exergy efficiency again rises due to further decrease in the solar radiation intensity and ambient temperature. The maximum value of measured instantaneous exergy efficiency was found to be 3.83% at 17:00 h and in time interval 09:00 h–15:00 h, it was 3.05% at 15:00 h. The theoretical instantaneous exergy efficiency was noticed to be increased in the same manner as theoretical instantaneous energy efficiency curve. The maximum value of theoretical instantaneous exergy efficiency was found to be 5.86% at 17:00 h. The r-value and e-value were found to be 0.979 and 29.38%, respectively for instantaneous exergy efficiency.

It has been observed from the Table 2, that the annual exergy output is higher for solar still with black cotton wick than solar still with jute wick at 1 cm and 2 cm water depths in every month. This is attributed to the higher distillate obtained with cotton wick in comparison to jute wick in the solar still. On the basis of annual energy and annual exergy, the energy payback time (EPBT), energy production factor (EPF), and life cycle conversion efficiency (LCCE) of the solar still with jute and black cotton wicks at 1 cm and 2 cm water depth have been evaluated and presented in Tables 7–8. The variation of energy payback time (EPBT) and energy production factor (EPF) for the solar still with jute and black cotton wicks at 1 cm water depth on the basis of annual energy and exergy is shown in Fig. 11. It has been observed that the EPBT is less for solar still with black cotton wick at 1 cm water depth on the basis of both annual energy and exergy gain. This is due to the margin between the embodied energy of solar still with jute and black cotton wicks were less, but the distillate and exergy gain value were higher for solar still with black cotton wick than jute wick significantly. So, EPBT is higher for solar still with jute wick on the basis of energy and exergy. The EPBT values has been found to be 0.692 and 0.637 years on the basis of energy; and 13.244 and 10.609 years on the basis of exergy with jute and black cotton wicks at 1 cm water depth, respectively. The EPBT values at 2 cm water depth has been found to be 0.749 and 0.698 years on the basis of energy; and 14.576 and 12.585 years on the basis of exergy with jute and black cotton wicks, respectively (Table 8).

Table 7
Energy payback time (EPBT), energy production factor (EPF), and life cycle conversion efficiency (LCCE) for the solar still with jute and black cotton wicks at 1 cm water depth based on annual energy and exergy.

Basis	Jute wick			Black cotton wick		
	EPBT (years)	EPF	LCCE	EPBT (years)	EPF	LCCE
Energy	0.692	1.443	0.079	0.637	1.568	0.103
Exergy	13.244	0.075	−0.178	10.609	0.094	−0.176

Table 8
Energy payback time (EPBT), energy production factor (EPF), and life cycle conversion efficiency (LCCE) for the solar still with jute and black cotton wicks at 2 cm water depth based on annual energy and exergy.

Basis	Jute wick			Black cotton wick		
	EPBT (years)	EPF	LCCE	EPBT (years)	EPF	LCCE
Energy	0.749	1.334	0.059	0.698	1.431	0.077
Exergy	14.576	0.068	−0.1776	12.585	0.079	−0.1771

Fig. 11 also shows the variation of energy production factor (EPF) for the solar still with jute and black cotton wicks at 1 cm water depth. It has been observed that the EPF is higher for solar still with black cotton wick on the energy and exergy basis. This is due to higher annual energy and exergy output with black cotton wick while the difference in embodied energy of the solar still with jute and black cotton wick is marginal. It means the rise in the numerator of Eqs. (53) and (54) is more than the rise in the denominator for solar still with black cotton wick in comparison to jute wick. Hence, the ratio is higher for solar still with black cotton wick. The EPF values has been found to be 1.443 and 1.568 on the basis of energy; and 0.075 and 0.094 on the basis of exergy with jute and black cotton wicks at 1 cm water depth, respectively (Table 7). The EPF values at 2 cm water depth has been found to be 1.334 and 1.431 on the basis of energy; and 0.068 and 0.079 on the basis of exergy with jute and black cotton wicks, respectively (Table 8).

Fig. 12 shows the variation of life cycle conversion efficiency (LCCE) with the life span ($n = 5$ to $n = 50$) of the solar still with jute and black cotton wicks at 1 cm water depth. The LCCE of the solar still with jute and black cotton wicks has been evaluated on the basis of energy and exergy and it has been noticed that the LCCE value increases with increase in lifetime or life span of the solar still. From Tables 7–8, one can be observed that the LCCE value for solar still with jute and black cotton wicks on the basis of exergy was found to be negative for the $n = 1$ year. This is mainly due to the difference between the annual exergy output and embodied energy in the numerator term of LCCE Eq. (56). The same observation has been noticed for the LCCE based on exergy for the solar still with jute and black cotton wicks at 1 cm water depth for $n = 5$ and 10 years (Table 9). The LCCE values has been found to be 0.255 and 0.280 on the basis of energy; and 0.010 and 0.014 on the basis of exergy

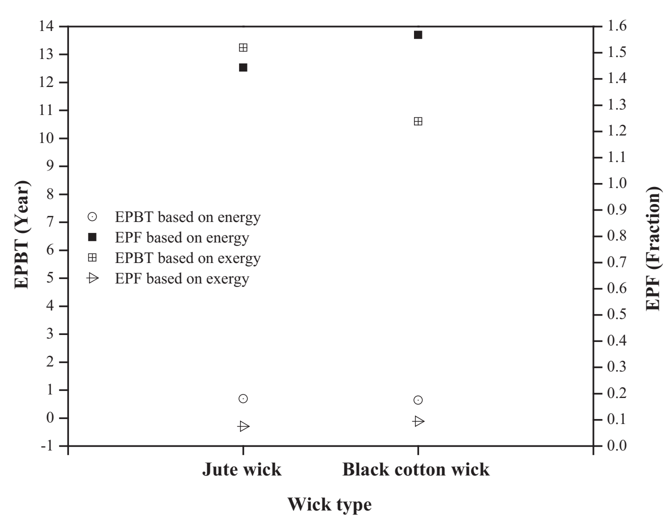

Fig. 11. Variation of energy payback time (EPBT) and energy production factor (EPF) for the solar still with jute and black cotton wicks at 1 cm water depth on annual energy and exergy basis.

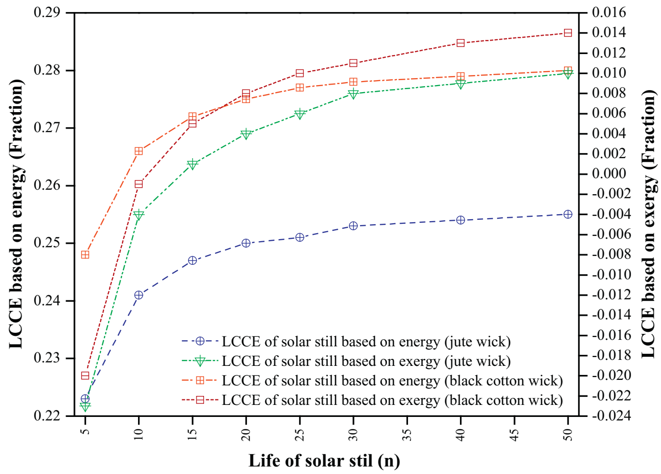

Fig. 12. Life cycle conversion efficiency (LCCE) of the solar still at 1 cm water depth for the life span of 50 years.

with jute and black cotton wicks, respectively for $n = 50$ years. Similarly, the LCCE values of the solar still with jute and black cotton wicks at 2 cm water depth can be calculated. On the basis of energy and exergy, the life cycle conversion efficiency (LCCE) of the solar still with jute and black cotton wicks at 1 cm water depth for the life span $n = 5$ to $n = 50$ years have been evaluated and presented in Table 9.

Table 9
Life cycle conversion efficiency (LCCE) of the solar still with jute and black cotton wicks at 1 cm water depth for life span of 50 years based on energy and exergy.

Years (n)	Jute wick		Black cotton wick	
	Energy	Exergy	Energy	Exergy
	LCCE	LCCE	LCCE	LCCE
5	0.223	−0.023	0.248	−0.020
10	0.241	−0.004	0.266	−0.001
15	0.247	0.001	0.272	0.005
20	0.250	0.004	0.275	0.008
25	0.251	0.006	0.277	0.010
30	0.253	0.008	0.278	0.011
40	0.254	0.009	0.279	0.013
50	0.255	0.010	0.280	0.014

The amount of CO_2 mitigated per annum (φ_{CO_2}) and environmental cost (carbon credits) has been evaluated for the solar still with jute and black cotton wicks at 1 cm and 2 cm water depth on the energy and exergy basis and presented in Table 10. It has been observed that the amount of CO_2 mitigated per annum has been found to be higher for solar still with black cotton wick at 1 cm water depth on the energy and exergy basis. This is attributed to the higher annual distillate yield obtained by the solar still with black cotton wick at 1 cm water depth. The CO_2 mitigated values has been found to be 7.82 and 8.69 tons of CO_2 on the basis of energy; and 0.155 and 0.198 tons of CO_2 on the basis of exergy with jute and black cotton wicks at 1 cm water depth, respectively. The CO_2 mitigated values at 2 cm water depth has been found to be 7.23 and 7.93 tons of CO_2 on the basis of energy; and 0.141 and 0.167 tons of CO_2 on the basis of exergy with jute and black cotton wicks, respectively (Table 10).

The environmental cost or carbon credits has also been found to be higher for solar still with black cotton wick at 1 cm water depth on the basis of energy and exergy. The carbon credits earned by the solar still with jute and black cotton wicks at 1 cm water depth has been found to be Rs. 6946.39 (86.78 €); Rs. 7721.03 (96.45 €), and Rs. 138.10 (1.72 €); Rs. 176.31 (2.20 €) on the basis of energy and exergy, respectively. The carbon credits earned by the solar still with jute and black cotton wicks at 2 cm water depth has been found to be Rs. 6418.70 (80.18 €); Rs. 7047.32 (88.04 €), and Rs. 125.48 (1.56 €); Rs. 148.62 (1.85 €) on the basis of energy and exergy, respectively (Table 10).

A detailed exergoeconomic analysis of the solar still with jute and black cotton wicks has been carried out and calculated values are presented in Tables 11–12. The capital recovery factor (CRF), sink fund factor (SFF), net present value (NPV), uniform annual cost (UAC), and exergoeconomic parameter (R_{ex}) of the solar still with jute and black cotton wicks at 1 cm water depth have been calculated for different life span (n = 30, 40, and 50 years) and interest rates (i = 4%, 8%, and 10%).

It has been observed that for the fixed life span of the solar still, NPV decreases with increase in the rate of interest while for fixed interest rate, NPV increases with the increase in life span of the system. The NPV has been found to be higher for solar still with black cotton wick than solar still with jute wick for a given interest rate and life span. One can also be noticed that for a fixed life span of the solar still, UAC rises with increase in the interest rate and for the fixed rate of interest, UAC decreases with increase in life span of the system. For a given rate of interest and life span, the UAC value has been found to be marginally higher for solar still with black cotton wick than the system with jute wick.

The exergy based exergoeconomic parameter has been calculated

Table 10
Enviroeconomic analysis of the solar still with jute and black cotton wicks at 1 cm and 2 cm water depth on the basis of thermal energy and exergy.

Environmental cost[a]									
Energy					Exergy				
Energy production cost		CO_2 mitigated (tons)	Environmental cost (carbon credits)		Exergy production cost		CO_2 mitigated (tons)	Environmental cost (carbon credits)	
(Rs.)	($)		(Rs.)	(€)	(Rs.)	($)		(Rs.)	(€)
1. Jute wick									
(a) 1 cm water depth									
7288.05	112.36	7.82	6946.39	86.78	381.30	5.87	0.155	138.10	1.72
(b) 2 cm water depth									
6734.40	103.82	7.23	6418.70	80.18	346.45	5.34	0.141	125.48	1.56
2. Black cotton wick									
(a) 1 cm water depth									
8100.80	124.89	8.69	7721.03	96.45	486.80	7.50	0.198	176.31	2.20
(b) 2 cm water depth									
7393.95	113.99	7.93	7047.32	88.04	410.35	6.32	0.167	148.62	1.85

[a] Average unit electricity cost is taken Rs. 5/kWh (0.07 US$ per kWh). 1 € = Indian Rs. 80.04 on 16/03/2018.

Table 11
Capital recovery factor, sink fund factor, net present value, uniform annual cost, and exergoeconomic parameter of the solar still with jute wick at 1 cm water depth.

Years (n)	Interest rate, i (%)	*CRF*	*SFF*	*NPV* (Rs.)	*UAC* (Rs.)	$E_{ex,ann}$ (kWh)	R_{ex} (kWh/Rs.)
30	4	0.0578	0.0178	22,574.65	1349.01	76.26	0.0565
40	4	0.0505	0.0105	24,118.40	1267.18	76.26	0.0601
50	4	0.0465	0.0065	25,161.30	1222.67	76.26	0.0623
30	8	0.0888	0.0088	19,731.04	1858.47	76.26	0.0410
40	8	0.0838	0.0038	20,194.90	1802.84	76.26	0.0423
50	8	0.0817	0.0017	20,409.75	1779.13	76.26	0.0428
30	10	0.1060	0.0060	19,053.20	2156.89	76.26	0.0353
40	10	0.1022	0.0022	19,386.54	2120.87	76.26	0.0359
50	10	0.1008	0.0009	19,486.34	2104.77	76.26	0.0362

for the solar still with jute and black cotton wicks at 1 cm water depth for the 30, 40, and 50 years life span. It has been noticed that the exergoeconomic parameter (R_{ex}) for the fixed life span of solar still reduces gradually with rise in the rate of interest for both the system with jute and black cotton wicks. For example, the R_{ex} values for 30 years of life time of solar still with black cotton wick has been found to be 0.0716, 0.0519, and 0.0447 kWh/Rs. with 4%, 8%, and 10% interest rate, respectively whereas it were 0.0565, 0.0410, and 0.0353 kWh/Rs. with the corresponding interest rates for the system with jute wick (n = 30 years). This is attributed to fact that the uniform annual cost (UAC) rises with the increase in rate of interest for the fixed lifetime of solar still. The R_{ex} values for the solar still with jute and black cotton wicks at 1 cm water depth have been found to be 0.0362, and 0.0458 kWh/Rs., respectively for 10% interest rate and 50 years life span of the system. In a similar manner, the exergoeconomic analysis of the solar still with jute and black cotton wicks at 2 cm water depth can be performed.

Table 12
Capital recovery factor, sink fund factor, net present value, uniform annual cost, and exergoeconomic parameter of the solar still with black cotton wick at 1 cm water depth.

Years (n)	Interest rate, i (%)	*CRF*	*SFF*	*NPV* (Rs.)	*UAC* (Rs.)	$E_{ex,ann}$ (kWh)	R_{ex} (kWh/Rs.)
30	4	0.0578	0.0178	22,729.16	1358.45	97.36	0.0716
40	4	0.0505	0.0105	24,275.34	1275.67	97.36	0.0763
50	4	0.0465	0.0065	25,319.88	1230.65	97.36	0.0791
30	8	0.0888	0.0088	19,890.63	1873.87	97.36	0.0519
40	8	0.0838	0.0038	20,355.78	1817.60	97.36	0.0535
50	8	0.0817	0.0017	20,571.23	1793.61	97.36	0.0542
30	10	0.1060	0.0060	19,213.81	2175.50	97.36	0.0447
40	10	0.1022	0.0022	19,548.00	2138.98	97.36	0.0455
50	10	0.1008	0.0009	19,648.13	2122.70	97.36	0.0458

Table 13
Energy and exergy input, and gain obtained for the solar still with jute and black cotton wicks at 1 cm and 2 cm water depth for 300 days in Allahabad (U.P.), India.

Particulars	Energy and exergy on annual basis (kWh) at 1 cm water depth		Energy and exergy on annual basis (kWh) at 2 cm water depth	
	Jute wick	Black cotton wick	Jute wick	Black cotton wick
Energy output (E_{out})	1213.52	1349.58	1121.09	1231.12
Solar energy input ($E_{sol(en)}$)	4617.47	4689.40	4663.65	4741.24
Exergy output (E_{ex})	64.90	82.35	59.22	69.52
Exergy input ($E_{sol(ex)}$)	4303.11	4370.80	4347.52	4418.25

Similarly, the energy matrices (EPBT, EPF, and LCCE), exergy; enviroeconomic; and exergoeconomic values have been obtained for 300 days in a year. The remaining 65 days are considered as fully cloudy or rainy days, in which the solar still is non–productive for the climatic condition of Allahabad (U.P.), India. The energy and exergy input and outputs for the solar still with jute and black cotton wicks at 1 cm and 2 cm water depth for 300 days of operation is presented in Table 13. The EPBT values has been found to be 0.832 and 0.765 years on the basis of energy; and 15.560 and 12.541 years on the basis of exergy with jute and black cotton wicks at 1 cm water depth, respectively. The EPF values at 1 cm water depth has been found to be 1.201 and 1.306 on the basis of energy; and 0.064 and 0.079 on the basis of exergy with jute and black cotton wicks, respectively. The LCCE values for solar still with jute and black cotton wicks at 1 cm water depth based on annual energy for 300 days of operation has been found to be 0.044 and 0.067, respectively whereas it was −0.219 and − 0.217, respectively on exergy basis. The CO_2 mitigated values at 1 cm water depth has been found to be 6.51 and 7.24 tons of CO_2 on the basis of energy; and 0.132 and 0.168 tons of CO_2 on the basis of exergy with jute and black cotton wicks, respectively. The carbon credits earned by the solar still with jute and black cotton wicks at 1 cm water depth has been found to be Rs. 5783.14 (72.24 €); Rs. 6431.57 (80.35 €), and Rs. 117.54 (1.47 €); Rs. 149.14 (1.86 €) on the basis of energy and exergy, respectively. The R_{ex} values for 300 days operation of the solar still with jute and black cotton wicks at 1 cm water depth have been found to be 0.030, and 0.038 kWh/Rs., respectively for 10% interest rate and 50 years life span of the system. A similar analysis can also be performed for 300 days operation of the solar still with jute and black cotton wicks at 2 cm water depth.

The comparison of the present analysis with the previous studies based on their energy matrices and capital investment is given in Table 14. Singh et al. [59] reported the EPBT and EPF of the conventional double slope passive solar distiller as 1.43 years and 0.70, respectively. The capital cost of the solar still was also higher due to its costly GRP body, which makes it uneconomical. Tiwari and Selim [42] designed the conventional double slope multi–wick solar still with FRP as a body material and jute cloth pieces as a wick. The layout of wicks (one upon another) leads to dry patches in the wicks due to improper supply of water into the wicks [57]. For the economic analysis of the FRP multi–wick solar still (conventional), one can be assumed the mass

Table 14
Comparison between present modified multi–wick basin type double slope solar still and conventional double slope solar stills.

Sr. no.	Type of solar still	Capital investment (US $)	Embodied energy (kWh)	Energy Matrices (Annual energy basis)		
				EPBT (years)	EPF	LCCE
1	Conventional double slope passive solar still [59]	357.41	1483.90	1.43	0.70	−0.124
2	Conventional double slope multi–wick solar still [42]	265.28	2212.55	1.38	0.724	−0.169
3	Modified multi–wick double slope solar still with jute wick at 1 cm water depth (present study)	215.82	1009.99	0.692	1.443	0.079
4	Modified multi–wick double slope solar still with black cotton wick at 1 cm water depth (present study)	218.32	1032.91	0.637	1.568	0.103

of components of the solar still (except jute cloth pieces) are same as that of conventional passive double slope solar distiller [59]. The capital cost of investment has been evaluated as 265.28 US$. The total embodied energy for the system has been evaluated as 2212.55 kWh. For the estimation of energy matrices, the average daily distillate yield, and annual solar energy retrieved by the solar still are assumed as 3.5 l/m^2 and 3601.63 kWh ($E_{sol(en),\ ann}$is taken as same as that of conventional passive double slope solar distiller [59]), respectively. The EPBT, EPF, and LCCE of that solar still were found to be 1.38 years, 0.724, and − 0.169, respectively. The capital cost investment for the presented solar still with jute and cotton wicks were found to be Rs. 14,000 (215.82 US$) and Rs. 14,162 (218.32 US$), respectively, which shows that the presented solar still is cost–effective. The lower EPBT and higher EPF values of the solar still also indicate that the solar still is effective under the climatic conditions of Allahabad, Uttar Pradesh (U.P.), India.

12. Conclusions

In the present study, a thermal model of modified multi–wick basin type double slope solar still (MMWBDSSS) has been developed and experimentally validated with theoretical results. This study then covers energy matrices, enviroeconomic, and exergoeconomic assessments of the solar still with jute and black cotton wicks on the basis of energy and exergy. The following conclusions can be drawn on the basis of this study:

- The proposed thermal model of the solar still has been validated well by the experimental observations for water, average temperature of east and west side spread strap layer of water–wick, and distillate yield.
- The maximum values of instantaneous energy and exergy efficiencies were found to be 35% at 17:00 h and 3.83% at 17:00 h, respectively, and in time duration 09:00 h–15:00 h, the higher values of instantaneous energy and exergy efficiencies were noticed to be 27.51% at 14:00 h and 3.05% at 15:00 h, respectively.
- The energy payback time (EPBT) of the solar still on annual energy and exergy basis have been found to be increased with the decrease in the number of clear days. EPBT values has been found to be 0.692 and 0.637 years on the basis of energy; and 13.244 and 10.609 years on the basis of exergy with jute and black cotton wicks at 1 cm water depth, respectively for 365 days operation of solar still, and it has been found to be 0.832 and 0.765 years on the basis of energy; and 15.560 and 12.541 years on the basis of exergy with jute and black cotton wicks at 1 cm water depth, respectively for 300 days operation.
- The energy production factor (EPF) values has been found to be 1.443 and 1.568 on the basis of energy; and 0.075 and 0.094 on the basis of exergy with jute and black cotton wicks at 1 cm water depth, respectively for 365 days operation, and it has been found to be 1.201 and 1.306 on the basis of energy; and 0.064 and 0.079 on the basis of exergy with jute and black cotton wicks at 1 cm water depth, respectively for 300 days operation.
- The life cycle conversion efficiency (LCCE) of the solar still increases with the increase in life span of the system.
- The amount of CO_2 emission mitigated per annum has been found to be 7.82 and 8.69 tons on the basis of energy; and 0.155 and 0.198 tons on the basis of exergy with jute and black cotton wicks at 1 cm water depth, respectively for 365 days operation, and it has been found to be 6.51 and 7.24 tons on the basis of energy; and 0.132 and 0.168 tons on the basis of exergy with jute and black cotton wicks at 1 cm water depth, respectively for 300 days operation.
- The environmental cost or carbon credits per annum earned by the solar still with jute and black cotton wicks at 1 cm water depth has been found to be Rs. 6946.39 (86.78 €); Rs. 7721.03 (96.45 €), and Rs. 138.10 (1.72 €); Rs. 176.31 (2.20 €) on the basis of energy and exergy, respectively for 365 days operation, and it has found to be Rs. 5783.14 (72.24 €); Rs. 6431.57 (80.35 €), and Rs. 117.54 (1.47 €); Rs. 149.14 (1.86 €) on the basis of energy and exergy with jute and black cotton wicks at 1 cm water depth, respectively for 300 days operation.
- The exergoeconomic parameter for the fixed life span of the solar still decreases with increase in the rate of interest and decrease in the number of clear days of operation for the system with jute and black cotton wicks.

Acknowledgement

The authors acknowledge with thanks the support extended by Solar Energy Laboratory, Mechanical Engineering Department, MNNIT Allahabad in conducting the experiments. The present work is carried out under the TEQIP–II fund sanctioned against letter Ref. no. 570/TEQIP–II/2017, dated: 22/02/2017 of Motilal Nehru National Institute of Technology Allahabad, Allahabad, Uttar Pradesh–211004, India.

Appendix A

Analytical expressions for vapor, inner walls, inner glass covers, and wicks (strap layer of water–wick) temperatures have been obtained in thermal modeling in terms of T_w

$$T_v = -\frac{A_1}{A_2} + \frac{T_w}{A_2} \qquad T_{iEg} = \left(\frac{R_1}{U_1} - \frac{h_{VEg}A_1}{U_1A_2}\right) + \frac{h_{VEg}}{U_1A_2}T_w$$

$$T_{iWg} = \left(\frac{R_2}{U_2} - \frac{h_{VWg}A_1}{U_2A_2}\right) + \frac{h_{VWg}}{U_2A_2}T_w \qquad T_{iW} = \left(\frac{R_3}{U_3} - \frac{h_{VW}A_1}{U_3A_2}\right) + \frac{h_{VW}}{U_3A_2}T_w$$

$$T_{iE} = \left(\frac{R_4}{U_4} - \frac{h_{VE}A_1}{U_4A_2}\right) + \frac{h_{VE}}{U_4A_2}T_w \qquad T_{iS} = \left(\frac{R_5}{U_5} - \frac{h_{VS}A_1}{U_5A_2}\right) + \frac{h_{VS}}{U_5A_2}T_w$$

$$T_{iN} = \left(\frac{R_6}{U_6} - \frac{h_{NV}A_1}{U_6A_2}\right) + \frac{h_{NV}}{U_6A_2}T_w \qquad T_{w-wick(E)} = \left(P_1 - \frac{A_1}{A_2}\right) + \frac{T_w}{A_2}$$

$$T_{w-wick(W)} = \left(P_2 - \frac{A_1}{A_2}\right) + \frac{T_w}{A_2} \qquad T_{w-wick(avg.)} = \frac{(T_{w-wick(E)} + T_{w-wick(W)})}{2}$$

Expressions for the terms *A_1, A_2, R_1, R_2, R_3, R_4, R_5, R_6, P_1, P_2, U_1, U_2, U_3, U_4, U_5, U_6, α_1, and α_2*

$$A_1 = \frac{-\left[\begin{array}{l}\frac{h_{NV}A_NR_6}{U_6} + \frac{h_{VS}A_SR_5}{U_5} + \frac{h_{VE}A_ER_4}{U_4} \\ + \frac{h_{VW}A_WR_3}{U_3} + \frac{h_{VWg}A_{Wg}R_2}{U_2} + \frac{h_{VEg}A_{Eg}R_1}{U_1} \\ + \beta\alpha'_{w-wick}A_{wick(E)}I_{Eg}(t) + \beta\alpha'_{w-wick}A_{wick(W)}I_{Wg}(t)\end{array}\right]}{h_{wv}A_b}$$

$$A_2 = \frac{\left[\begin{array}{l}\left(\begin{array}{l}h_{wv}A_b + h_{NV}A_N + h_{VS}A_S + h_{VE}A_E \\ +h_{VW}A_W + h_{VEg}A_{Eg} + h_{VWg}A_{Wg}\end{array}\right) - \\ \left(\begin{array}{l}\frac{h_{NV}A_N}{U_6} + \frac{h_{VS}A_S}{U_5} + \frac{h_{VE}A_E}{U_4} \\ + \frac{h_{VW}A_W}{U_3} + \frac{h_{VWg}A_{Wg}}{U_2} + \frac{h_{VEg}A_{Eg}}{U_1}\end{array}\right)\end{array}\right]}{h_{wv}A_b}$$

$$P_1 = \frac{\beta\alpha'_{w-wick}I_{Eg}(t)}{h_{w-wick(E)}} \qquad P_2 = \frac{\beta\alpha'_{w-wick}I_{Wg}(t)}{h_{w-wick(W)}}$$

$R_1 = \alpha_g' I_{Eg}(t) + h_{go}T_a$ $R_2 = \alpha_g' I_{Wg}(t) + h_{go}T_a$
$R_3 = \alpha_W' I_W(t) + h_{acro}T_a$ $R_4 = \alpha_E' I_E(t) + h_{acro}T_a$
$R_5 = \alpha_S' I_S(t) + h_{acro}T_a$ $R_6 = \alpha_N' I_N(t) + h_{FRPo}T_a$
$U_1 = h_{VEg} + h_{go}$ $U_2 = h_{VWg} + h_{go}$
$U_3 = h_{VW} + h_{acro}$ $U_4 = h_{VE} + h_{acro}$
$U_5 = h_{VS} + h_{acro}$ $U_6 = h_{NV} + h_{FRPo}$

$$\alpha_1 = (1-\beta)\begin{bmatrix}\alpha'_{wg}A_b\{I_{Eg}(t) + I_{Wg}(t)\}\\ + \alpha'_{wacr}A_b\{I_E(t) + I_W(t) + I_S(t)\}\end{bmatrix} \qquad \alpha_2 = (1-\beta)\begin{bmatrix}\alpha'_{bg}A_b\{I_{Eg}(t) + I_{Wg}(t)\}\\ + \alpha'_{bacr}A_b\{I_E(t) + I_W(t) + I_S(t)\}\end{bmatrix}$$

Expressions used to calculate different heat transfer coefficients in thermal modeling

$$h_{go} = \left[\frac{1}{h_{Kg}} + \frac{1}{h_o}\right]^{-1} \qquad h_{acro} = \left[\frac{1}{h_{Kacr}} + \frac{1}{h_o}\right]^{-1}$$

$$h_{FRPo} = \left[\frac{1}{h_{KFRP}} + \frac{1}{h_o}\right]^{-1} \qquad h_{Kg} = k_g/l_g$$

$$h_{Kacr} = k_{acr}/l_{acr} \qquad h_{KFRP} = k_{FRP}/l_{FRP}$$

$$h_{VE} = \begin{bmatrix}0.884\left[(T_V - T_{iE}) + \dfrac{(P_V - P_{iE})(T_V + 273)}{(268.9\times 10^3 - P_V)}\right]^{1/3}\\ + \varepsilon_{eff}\sigma[(T_V + 273)^2 + (T_{iE} + 273)^2][T_V + T_{iE} + 546]\end{bmatrix} \qquad h_{VW} = \begin{bmatrix}0.884\left[(T_V - T_{iW}) + \dfrac{(P_V - P_{iW})(T_V + 273)}{(268.9\times 10^3 - P_V)}\right]^{1/3}\\ + \varepsilon_{eff}\sigma[(T_V + 273)^2 + (T_{iW} + 273)^2][T_V + T_{iW} + 546]\end{bmatrix}$$

$$h_{NV} = \begin{bmatrix}0.884\left[(T_{iN} - T_V) + \dfrac{(P_{iN} - P_V)(T_{iN} + 273)}{(268.9\times 10^3 - P_{iN})}\right]^{1/3}\\ + \varepsilon_{eff}\sigma[(T_{iN} + 273)^2 + (T_V + 273)^2][T_{iN} + T_V + 546]\end{bmatrix} \qquad h_{VEg} = \begin{bmatrix}0.884\left[(T_V - T_{iEg}) + \dfrac{(P_V - P_{iEg})(T_V + 273)}{(268.9\times 10^3 - P_V)}\right]^{1/3}\\ + \varepsilon_{eff}\sigma[(T_V + 273)^2 + (T_{iEg} + 273)^2][T_V + T_{iEg} + 546]\end{bmatrix}$$

$$h_{VWg} = \begin{bmatrix}0.884\left[(T_V - T_{iWg}) + \dfrac{(P_V - P_{iWg})(T_V + 273)}{(268.9\times 10^3 - P_V)}\right]^{1/3}\\ + \varepsilon_{eff}\sigma[(T_V + 273)^2 + (T_{iWg} + 273)^2][T_V + T_{iWg} + 546]\end{bmatrix} \qquad h_{w-wick(avg.)} = \frac{(h_{w-wick(E)} + h_{w-wick(W)})}{2}$$

$$h_{wv} = \begin{bmatrix}\left[(0.016273)\left(0.884\begin{bmatrix}(T_w - T_V)\\ + \dfrac{(P_w - P_V)(T_w + 273)}{(268.9\times 10^3 - P_w)}\end{bmatrix}^{1/3}\right)\left(\dfrac{P_w - P_V}{T_w - T_V}\right)\right]\\ + \left[0.884\left(\left[(T_w - T_V) + \dfrac{(P_w - P_V)(T_w + 273)}{(268.9\times 10^3 - P_w)}\right]^{1/3}\right)\right] + \varepsilon_{eff}\sigma[(T_w + 273)^2 + (T_V + 273)^2][T_w + T_V + 546]\end{bmatrix}$$

Partial saturated vapor pressure at water, vapor, inside walls, and wicks (strap layer of wick) temperature [60,61]

$$P_w = \exp\left[25.317 - \frac{5144}{(T_w + 273)}\right] \qquad P_V = \exp\left[25.317 - \frac{5144}{(T_V + 273)}\right]$$

$$P_{iE} = \exp\left[25.317 - \frac{5144}{(T_{iE} + 273)}\right] \qquad P_{iW} = \exp\left[25.317 - \frac{5144}{(T_{iW} + 273)}\right]$$

$$P_{iN} = \exp\left[25.317 - \frac{5144}{(T_{iN} + 273)}\right] \qquad P_{iS} = \exp\left[25.317 - \frac{5144}{(T_{iS} + 273)}\right]$$

$$P_{iEg} = \exp\left[25.317 - \frac{5144}{(T_{iEg} + 273)}\right] \qquad P_{iWg} = \exp\left[25.317 - \frac{5144}{(T_{iWg} + 273)}\right]$$

$$P_{w-wick(E)} = \exp\left[25.317 - \frac{5144}{(T_{w-wick(E)} + 273)}\right] \qquad P_{w-wick(W)} = \exp\left[25.317 - \frac{5144}{(T_{w-wick(W)} + 273)}\right]$$

Coefficient of correlation (r–value) [67]

$$r = \frac{n\sum x_i y_i - \sum(x_i)\sum(y_i)}{\sqrt{n\sum x_i^2 - (\sum x_i)^2}\sqrt{n\sum y_i^2 - (\sum y_i)^2}}$$

Root mean square percentage deviation (e–value) [67]

$$e = \sqrt{\frac{\sum(e_i)^2}{n}}$$

where, x_i is theoretical value obtained from the thermal modeling and y_i is experimental data.

and $e_i = \left[\frac{x_i - y_i}{x_i}\right] \times 100$ and $i = 1$ to n (number of observations).

References

[1] A.G.M. Ibrahim, A.M. Rashad, I. Dincer, Exergoeconomic analysis for cost optimization of a solar distillation system, Sol. Energy 151 (2017) 22–32.
[2] H.T. El–Dessouky, H.M. Ettouney, Fundamentals of Salt Water Desalination, Elsevier, 2002.
[3] V.G. Gude, N. Nirmalakhandan, S. Deng, Renewable and sustainable approaches for desalination, Renew. Sust. Energ. Rev. 14 (2010) 2641–2654.
[4] A. Trad, A. Kaabi, Effect of orientation on the performance of a symmetric solar still with a double effect solar still (comparison study), Desalination 329 (2013) 68–77.
[5] T. Arunkumar, R. Jayaprakash, D. Denkenberger, A. Ahsan, M.S. Okundamiya, S. Kumar, H. Tanaka, H.S. Aybar, An experimental study on a hemispherical solar still, Desalination 286 (2012) 342–348.
[6] R. Sathyamurthy, H.J. Kennady, P.K. Nagarajan, A. Ahsan, Factors affecting the performance of triangular pyramid solar still, Desalination 344 (2014) 383–390.
[7] T. Rajaseenivasan, K.K. Murugavel, Theoretical and experimental investigation on double basin double slope solar still, Desalination 319 (2013) 25–32.
[8] P.U. Suneesh, R. Jayaprakash, T. Arunkumar, D. Denkenberger, Effect of air flow on "V" type solar still with cotton gauze cooling, Desalination 337 (2014) 1–5.
[9] H.E. Gad, S.S. El-Din, A.A. Hussien, K. Ramzy, Analysis of a conical solar still performance: an experimental study, Sol. Energy 122 (2015) 900–909.
[10] A.S. Abdullah, Improving the performance of stepped solar still, Desalination 319 (2013) 60–65.
[11] F.T. Farshad, M. Dashtban, M. Hamid, Experimental investigation of a weir–type cascade solar still with built–in latent heat energy storage system, Desalination 260

(2010) 248–253.
[12] A. Ahsan, T. Fukuhara, Mass and heat transfer model of tubular solar still, Sol. Energy 84 (2010) 1147–1156.
[13] T. Arunkumar, R. Velraj, D. Denkenberger, R. Sathyamurthy, K. Vinothkumar, K. Porkumaran, A. Ahsan, Effect of heat removal on tubular solar desalting system, Desalination 379 (2016) 24–33.
[14] T. Arunkumar, R. Velraj, D.C. Denkenberger, R. Sathyamurthy, K.V. Kumar, A. Ahsan, Productivity enhancements of compound parabolic concentrator tubular solar stills, Renew. Energy 88 (2016) 391–400.
[15] S. Gorjian, B. Ghobadian, T.T. Hashjin, A. Banakar, Experimental performance evaluation of a stand–alone point–focus parabolic solar still, Desalination 352 (2014) 1–17.
[16] N. Rahbar, J.A. Esfahani, Experimental study of a novel portable solar still by utilizing the heatpipe and thermoelectric module, Desalination 284 (2012) 55–61.
[17] N. Rahbar, J.A. Esfahani, A. Asadi, An experimental investigation on productivity and performance of a new improved design portable asymmetrical solar still utilizing thermoelectric modules, Energy Convers. Manag. 118 (2016) 55–62.
[18] V. Velmurugan, M. Gopalakrishnan, R. Raghu, K. Srithar, Single basin solar still with fin for enhancing productivity, Energy Convers. Manag. 49 (2008) 2602–2608.
[19] V. Velmurugan, C. Deenadayalan, H. Vinod, K. Srithar, Desalination of effluent using fin type solar still, Energy 33 (2008) 1719–1727.
[20] Z. Omara, M.H. Hamed, A. Kabeel, Performance of finned and corrugated absorbers solar stills under Egyptian conditions, Desalination 277 (2011) 281–287.
[21] H. Tanaka, Experimental study of a basin type solar still with internal and external reflectors in winter, Desalination 249 (2009) 130–134.
[22] Z. Omara, A. Kabeel, M. Younes, Enhancing the stepped solar still performance using internal and external reflectors, Energy Convers. Manag. 78 (2014) 876–881.
[23] H. Ali, Effect of forced convection inside the solar still on heat and mass transfer coefficients, Energy Convers. Manag. 34 (1993) 73–79.
[24] H. Ali, Experimental study on air motion effect inside the solar still on still performance, Energy Convers. Manag. 32 (1991) 67–70.
[25] D.D.W. Rufuss, S. Iniyan, L. Suganthi, P.A. Davies, Solar stills: a comprehensive review of designs, performance and material advances, Renew. Sust. Energ. Rev. 63 (2016) 464–496.
[26] J.A. Eibling, S.G. Talbert, G.O.G. Lof, Solar stills for community use – digest of technology, Sol. Energy 13 (1971) 263–276.
[27] H.P. Garg, H.S. Mann, Effect of climatic, operational and design parameters on the year round performance of single–sloped and double–sloped solar still under Indian arid zone conditions, Sol. Energy 18 (1976) 159–163.
[28] M.A.S. Malik, G.N. Tiwari, A. Kumar, M.S. Sodha, Solar Distillation, first ed., Pregamon Press, UK, 1982.
[29] G.N. Tiwari, Recent advances in solar distillation, in: K. Raj, K.P. Maheshwari, R.L. Sawhney (Eds.), Solar Energy and Energy Conservation, Wiley, Eastern, New Delhi, 1992, pp. 32–149 (Chap. 2).
[30] G.N. Tiwari, H.N. Singh, R. Tripathi, Present status of solar distillation, Sol. Energy 75 (2003) 367–373.
[31] N. Rahbar, J.A. Esfahani, Productivity estimation of a single–slope solar still: theoretical and numerical analysis, Energy 49 (2013) 289–297.
[32] N. Rahbar, J.A. Esfahani, E. Fotouhi–Bafghi, Estimation of convective heat transfer coefficient and water–productivity in a tubular solar still–CFD simulation and theoretical analysis, Sol. Energy 113 (2015) 313–323.
[33] N. Rahbar, J.A. Esfahani, Estimation of convective heat transfer coefficient in a single – slope solar still: a numerical study, Desalin. Water Treat. 50 (2012) 387–396.
[34] R. Dev, G.N. Tiwari, Characteristic equation of a passive solar still, Desalination 245 (2009) 246–265.
[35] R. Dev, H.N. Singh, G.N. Tiwari, Characteristic equation of double slope passive solar still, Desalination 267 (2011) 261–266.
[36] S.K. Shukla, V.P.S. Sorayan, Thermal modelling of solar stills: an experimental validation, Renew. Energy 30 (2005) 683–699.
[37] V.K. Dwivedi, G.N. Tiwari, Comparison of internal heat transfer coefficients in passive solar stills by different thermal models: an experimental validation, Desalination 246 (2009) 304–318.
[38] A.O. Al–Sulttani, A. Ahsan, A. Rahman, N.N. Nik Daud, S. Idrus, Heat transfer coefficients and yield analysis of a double–slope solar still hybrid with rubber scrapers: an experimental and theoretical study, Desalination 407 (2017) 61–74.
[39] A.K. Tiwari, G.N. Tiwari, Effect of cover inclination and water depth on performance of a solar still for Indian climatic conditions, J. Sol. Energy Eng. 130 (2008) 1–4.
[40] L. Sahota, G.N. Tiwari Shyam, Energy matrices, enviroeconomic and exergoeconomic analysis of passive double slope solar still with water based nanofluids, Desalination 409 (2017) 66–79.
[41] M.S. Sodha, A. Kumar, G.N. Tiwari, R.C. Tyagi, Simple multiple wick solar still analysis and performance, Sol. Energy 26 (1981) 127–131.
[42] G.N. Tiwari, G.A.M. Selim, Double slope fibre reinforced plastic (FRP) multiwick solar still, Solar Wind Technol. 1 (4) (1984) 229–235.
[43] S.H. Sengar, A.G. Mohod, Y.P. Khandetod, S.P. Modak, D.K. Gupta, Design and development of wick type solar distillation system, J. Soil Sci. Environ. Manag. 2 (7) (2011) 125–133.
[44] A.N. Minasian, A.A. Al–Karaghouli, An improved solar still: the wick–basin type, Energy Convers. Manag. 36 (3) (1995) 213–217.
[45] A.A. Al–Karaghouli, A.N. Minasian, A floating–wick type solar still, Renew. Energy 6 (1) (1995) 77–79.
[46] K. Ohshiro, T. Noscco, T. Nagata, A compact solar still utilizing hydrophobic poly (tetrafluoroethylene) nets for separating neighbouring wicks, Desalination 105 (1996) 207–217.
[47] N.K. Dhiman, G.N. Tiwari, Effect of water flowing over the glass of a multi–wick solar still, Energy Convers. Manag. 30 (3) (1990) 245–250.
[48] B. Janarthanan, J. Chandrasekaran, S. Kumar, Evaporative heat loss and heat transfer for open–and closed–cycle systems of a floating tilted wick solar still, Desalination 180 (2005) 291–305.
[49] B. Janarthanan, J. Chandrasekaran, S. Kumar, Performance of floating cum tilted–wick type solar still with the effect of water flowing over the glass cover, Desalination 190 (2006) 51–62.
[50] H. Tanaka, Y. Nakatake, Improvement of the tilted wick solar still by using a flat plate reflector, Desalination 216 (2007) 139–146.
[51] H. Tanaka, Y. Nakatake, Increase in distillate productivity by inclining the flat plate external reflector of a tilted wick solar still in winter, Sol. Energy 83 (2009) 785–789.
[52] H. Tanaka, Y. Nakatake, One step azimuth tracking tilted–wick solar still with a vertical flat plate reflector, Desalination 235 (2009) 1–8.
[53] H. Tanaka, Tilted wick solar still with flat plate bottom reflector, Desalination 273 (2011) 405–413.
[54] H. Tanaka, Tilted wick solar still with external flat plate reflector: optimum inclination of still and reflector, Desalination 249 (2009) 411–415.
[55] A.E. Kabeel, Performance of solar still with concave wick evaporation surface, Energy 34 (2009) 1504–1509.
[56] K.K. Murugavel, Kn.K.S.K. Chockalingam, K. Srithar, An experimental study on single basin double slope simulation solar still with thin layer of water in the basin, Desalination 220 (2008) 687–693.
[57] P. Pal, P. Yadav, R. Dev, D. Singh, Performance analysis of modified basin type double slope multi–wick solar still, Desalination 422 (2017) 68–82.
[58] P. Pal, A.K. Nayak, R. Dev, A modified double slope basin type solar distiller: experimental and enviro–economic study, Evergreen 5 (1) (2018) 52–61.
[59] D.B. Singh, G.N. Tiwari, I.M. Al–Helal, V.K. Dwivedi, J.K. Yadav, Effect of energy matrices on life cycle cost analysis of passive solar stills, Sol. Energy 134 (2016) 9–22.
[60] G.N. Tiwari (Ed.), Solar Energy – Fundamentals, Design, Modeling and Applications, revised ed., Narosa Publishing House, New Delhi (India), 2013.
[61] G.N. Tiwari, A. Tiwari, Solar Distillation Practice for Water Desalination Systems, India, Anamaya, New Delhi, 2007.
[62] R. Dev, Thermal Modeling and Characteristic Equations for Passive and Active Solar Stills (Ph.D. Thesis), Centre for energy studies, IIT Delhi, 2012.
[63] K.R. Ranjan, S.C. Kaushik, Energy, exergy and thermo–economic analysis of solar distillation systems: a review, Renew. Sust. Energ. Rev. 27 (2013) 709–723.
[64] R. Petela, Exergy of undiluted thermal radiation, Sol. Energy 86 (2003) 241–247.
[65] G.N. Tiwari, V. Dimri, A. Chel, Parametric study of an active and passive solar distillation system: energy and exergy analysis, Desalination 242 (2009) 1–18.
[66] E.K. Akpinar, Drying of mint leaves in a solar dryer and under open sun: modelling, performance analyses, Energy Convers. Manag. 51 (2010) 2407–2418.
[67] S.C. Chapra, R.P. Canale, Numerical Methods for Engineers, 4th ed., McGraw Hill Publication, New York, 2002.
[68] G.N. Tiwari, R.K. Mishra, Advanced Renewable Energy Sources, RSC Publishing Cambridge, UK, 2012.
[69] B.K. Sovacool, Valuing the greenhouse gas emissions from nuclear power: a critical survey, Energy Policy 36 (2008) 2940–2953.
[70] B.J. Huang, T.H. Lin, W.C. Hung, F.S. Sun, Performance evaluation of solar photovoltaic/thermal systems, Sol. Energy 70 (2001) 443–448.
[71] S. Agrawal, G.N. Tiwari, Enviroeconomic analysis and energy matrices of glazed hybrid photovoltaic module air collector, Sol. Energy 92 (2013) 139–146.
[72] A. Chel, G.N. Tiwari, Thermal performance and embodied energy analysis of a passive house–case study of vault roof mud–house in India, Appl. Energy 86 (2009) 1956–1969.
[73] H. Sharon, K.S. Reddy, D. Krithika, L. Philip, Experimental performance investigation of tilted solar still with basin and wick for distillate quality and enviro–economic aspects, Desalination 410 (2017) 30–54.